Modeling corticotroph deficiency with pituitary organoids supports the functional role of *NFKB2* in human pituitary differentiation

Authors

Thi Thom Mac[1, 2], Teddy Fauquier[1], Nicolas Jullien[3], Pauline Romanet[1, 4], Heather C. Etchevers[1], Anne Barlier[1, 4, 5], Frederic Castinetti[1, 5], Thierry Brue[1, 5*]*

(1) Aix Marseille Univ, INSERM, UMR1251, Marseille Medical Genetics, Institut MarMaRa, Marseille, France

(2) Endocrinology Department, Hanoi Medical University Hospital, Hanoi, Vietnam

(3) Aix Marseille Univ, CNRS, UMR7051, Institut de NeuroPhysiopathologie, Marseille, France

(4) Aix Marseille Univ, APHM, INSERM, MMG, Laboratory of Molecular Biology, La Conception Hospital, Institut MarMaRa, Marseille, France

(5) Aix Marseille Univ, APHM, INSERM, MMG, Department of Endocrinology, La Conception Hospital, Institut MarMaRa, Marseille, France

Keywords

Congenital hypopituitarism, DAVID syndrome, hiPSC, CRISPR/Cas9, organoids, NFKB2, anterior pituitary deficiency, ACTH deficiency, corticotroph, differentiation, stem cell, development, hypogammaglobulinemia, CVID, variable immunodeficiency

*** Corresponding authors**

Prof. Thierry Brue, La Conception Hospital, Department of Endocrinology, 147 boulevard Baille, 13005 Marseille, France; thierry.brue@ap-hm.fr

Dr. Teddy Fauquier, Aix Marseille Univ, INSERM, UMR1251, Marseille Medical Genetics, Institut MarMaRa, Marseille, France ; teddy.fauquier@univ-amu.fr

Abstract

Background : Deficient Anterior pituitary with common Variable Immune Deficiency (DAVID) syndrome, combining adrenocorticotropic hormone deficiency (ACTHD) and primary hypogammaglobulinemia, is caused by *NFKB2* heterozygous mutations. Nuclear factor kappa B (NFKB) signaling is a key regulator of the immune system; however, the underlying mechanism of its association with endocrine symptoms remains unknown. The role of NFKB2 in the development of the human pituitary was called into question by *Nfkb2*-deficient *Lym1* mice, which have normal pituitary functions.

Purpose : The aim of this study was to create a human disease model to define the role of *NFKB2* in human pituitary development.

Methods: We established pituitary organoids in three-dimensional (3D) culture after directed differentiation from CRISPR/Cas9-edited human induced pluripotent stem cells (hiPSC). First, we conducted a proof-of-concept study, introducing a homozygous $TBX19^{K146R/K146R}$ missense pathogenic variant in hiPSC, an allele found in patients with congenital isolated ACTHD. We then used the same method to produce $NFKB2^{D865G/D865G}$ mutant organoids, harboring the pathogenic missense variant previously identified in DAVID patients. This mutation causes a failure of NFKB2 p100 phosphorylation that blocks processing to form active NFKB2 p52. We further characterized pituitary organoid development with bulk RNA sequencing and validated findings with quantitative RT-PCR and by immunofluorescence in section and whole organoids.

Results: Analysis of wild-type (WT) organoids demonstrated that this *in vitro* model recapitulates corticotroph cell differentiation. $TBX19^{K146R/K146R}$ organoids conserved early expression of *HESX1*, but had significantly decreased *PITX1*, *TBX19*, *LHX3,* and *POMC* transcription. $NFKB2^{D865G/D865G}$ organoids also had dramatically reduced corticotrophs. Furthermore, $NFKB2^{D865G/D865G}$ significantly perturbs the expression of 67 genes known to contribute to pituitary development, among which 39 transcription factors. Differential expression was found for several growth factor genes or genes associated with the epithelial-to-mesenchymal transition and terminal endocrine differentiation.

Conclusion: We used a combination of CRISPR/Cas9 editing and refinement of a 3D organoid culture protocol to model human ACTHD due to *TBX19* or *NFKB2* mutations. The *NFKB2* variant studied induced a significant decrease in corticotroph differentiation, confirming the causative role of NFKB2 in isolated or syndromic ACTHD and demonstrating for the first time a direct functional role of NFKB2 in human pituitary development.

Introduction

Adrenocorticotropic hormone deficiency (ACTHD) is defined by an insufficient production of ACTH by the pituitary, and then low adrenal cortisol production. Proper diagnosis and management of ACTHD is crucial as it is a life-threatening condition in the neonatal period characterized by hypoglycemia, cholestatic jaundice and seizures[1]. Constitutional ACTHD, i.e, ACTHD diagnosed at birth or during the first years of life, can be isolated or associated with other pituitary hormone deficiencies, such as growth hormone (GH) or thyrotropin-stimulating hormone (TSH), then as part of combined pituitary hormone deficiency (CPHD). ACTHD can be due to mutations in genes coding for transcription factors responsible for pituitary ontogenesis, especially the T-box transcription factor *TBX19* (also known as *TPIT*), *NFKB2*, *LHX3*, *LHX4*, *PROP1*, *HESX1*, *SOX2*, *SOX3*, *OTX2 and FGF8*.

Mutations of *TBX19* account for approximately two-thirds of neonatal-onset complete isolated ACTHD[1]. TBX19 is a T-box transcription factor restricted to pituitary pro-opiomelanocortin (POMC)-expressing cells in mice and humans. It is essential for *POMC* gene transcription and terminal differentiation of POMC-expressing cells[2]. POMC is the precursor of ACTH. *Tbx19*-deficient mice have only a few pituitary *Pomc*-expressing cells, with very low ACTH and undetectable corticosterone levels[3]. In humans with isolated ACTH deficiency, *TBX19* mutations lead to loss-of-function by different mechanisms, such as the *K146R* (exon 2, c.437 A>G) pathogenic variant located in the T-box region, which results in a loss of DNA-binding ability[1].

Thanks to GENHYPOPIT[4–6], an international network aimed at identifying new genetic etiologies of combined pituitary hormone deficiency, we described the first cases of DAVID (Deficient Anterior pituitary with common Variable Immune Deficiency) syndrome, a rare association of hypopituitarism (mainly ACTHD) and immune deficiency (hypogammaglobulinemia) [7]. DAVID syndrome is associated with variants in the nuclear factor kappa-B subunit 2 (*NFKB2*) gene[8,9]. In particular, we reported that a pathogenic, heterozygous D865G (exon 23, c.2594 A>G) *NFKB2* variant was found in a patient presenting with severe recurrent infections from 2 years of age, who at the age of 5 was diagnosed with ACTHD[7]. Mutations in the C-terminal region of NFKB2 lead to the disruption of both non-canonical and canonical pathways[10–12]. Full-length NFKB2 (p100) protein has 2 critical serines, S866 and S870, in the C-terminal domain. Phosphorylation of these sites yields the transcriptionally active NFKB2 (p52) through proteasomal processing of p100 protein. The D865G mutation, located adjacent to the critical S866 phosphorylation site, protects mutant protein from proteasomal degradation, causes defective processing of p100 to p52, and results in reduced translocation of p52 to the nucleus[8,11,12]. $NFKB2^{+/D865G}$ resulted in 50% of normal processing to p52, whereas $NFKB2^{D865G/D865G}$ exhibited near-absence of p52[12]. The nuclear factor kappa B (NFKB) signaling pathway is a known key regulator of the immune system[12–14], which likely explains the immune phenotype of patients with DAVID syndrome, including susceptibility to infections and auto-immune disorders[15]. In contrast, the underlying mechanism causing pituitary disorders remains unknown, with two predominating hypotheses: an indirect autoimmune hypophysitis, preferentially affecting corticotroph function, or a primary developmental defect suggested by the expression of *NFKB2* in the developing human pituitary[16]. However, a developmental role for *NFKB2* was not confirmed in the mouse: the *Lym1* mouse model carrying a

homozygous nonsense variant Y868* presented an apparently normal pituitary development and function[9].

Over the last years, human induced pluripotent stem cell (hiPSC)-derived organoids have emerged as promising models to study many developmental mechanisms and their perturbation in disease[17]. Pioneering work on human embryonic stem cells and later, hiPSC, has established that 3D organoid models can replicate aspects of pituitary development[18–20], and could thus be of major interest in modeling pituitary disorders[18,21,22]. In the present study, we applied recent progress in genome editing using CRISPR/Cas9[23] to a refined protocol to derive 3D organoids from hiPSC in order to model ACTHD. We validated the recapitulation of corticotroph cell differentiation *in vitro* by introducing a *TBX19* mutation known to induce isolated human ACTHD and documenting the subsequent deficiencies in corticotroph development. When our model was used to characterize the D865G *NFKB2* variant found in patients with DAVID syndrome, it displayed dramatically altered corticotroph differentiation in the absence of immune cells, clearly demonstrating for the first time a direct role of *NFKB2* in human pituitary development.

Materials and methods

Culture and maintenance of hiPSC lines

The 10742L healthy individual-derived hiPSC line was used in the study as the WT control (provided by the Cell Reprogramming and Differentiation Facility [MaSC], Marseille Medical Genetics, Marseille, France). Information about this hiPSC line is indicated in **Suppl. Table S1**. Two "knock-in" mutant lines carrying *TBX19*$^{K146R/K146R}$ (thereafter also designated as *TBX19* KI) and *NFKB2*$^{D865G/D865G}$ (thereafter also abridged as *NFKB2* KI) were generated using CRISPR/Cas9 editing from the isogenic control line. All hiPSC lines were cultured on six-well plates (Corning, #3335, New York, USA) coated with Synthemax II-SC Substrate (working concentration at 0.025 mg/mL, Corning, New York, USA) and maintained undifferentiated in a chemically defined growth medium (StemMACs hiPSC-Brew XF human medium; MACS Miltenyi Biotec, Paris, France)[24]. hiPSC lines were maintained in a humidified incubator under conditions of 37°C, 5% CO_2, with a daily change of medium, and passaged when cells reached 60-80 % confluency using enzyme-free ReleSR according to manufacturer's recommendations (StemCell Technologies, Canada, #05872).

CRISPR/Cas9 mediated genome editing of hiPSC

CRISPR/Cas9 gene editing was used to create the *TBX19*$^{K146R/K146R}$ and the *NFKB2*$^{D865G/D865G}$ mutations using the method as previously described[25].

CRISPR/Cas9 was used to generate two mutant hiPSC lines from 10742L hiPSC:

1) The *TBX19*$^{K146R/K146R}$ line, harboring the c.437A>G, p.Lys146Arg *TBX19* (NM_005149) pathogenic missense variant[1].

2) The *NFKB2*$^{D865G/D865G}$ line, harboring the c.2594A>G, p.Asp865Gly *NFKB2* (NM_001322934) pathogenic missense variant.

Preparation of the CRISPR/Cas9 sgRNA plasmid

For each targeted gene, sgRNA plasmid was prepared as previously described[26]. Briefly, we designed a sgRNA sequence within 20 nucleotides from the target site selected with the open-source CRISPOR tool (http://crispor.tefor.net/)[27].

The sgRNA sequence used to generate *TBX19*^{K146R} was (5'>3'): AAGCTGACCAACAAGCTCAA (see also Table S2).
The sgRNA sequence used to generate *NFKB2*^{D865G} was (5'>3'): GTGAAGGAAGACAGTGCGTA (see also Table S3).

We used the cAB03 (also known as pX459-pEF1alpha) vector as previously described[25]. Briefly, pSpCas9 (BB)-2A-Puro (PX459) V2.0 (Addgene plasmid # 62988, Addgene, Teddington, UK) was modified by the EF1 alpha promoter[25]. The chosen sgRNA was cloned into the cAB03 open plasmid vector using the method previously described by Arnaud et al[25]. The final vector expressed the corresponding sgRNA under the control of the U6 promoter, as well as *Cas9* under the control of the EF-1alpha promoter, and a puromycin resistance gene.

Single-stranded oligo DNA nucleotides (ssODN) design

We also designed donor sequences to generate *TBX19*^{K146R} and *NFKB2*^{D865G} missense mutations. A donor sequence is used for homology-directed repair, allowing the introduction ("knock-in", KI) of single nucleotide variations, with low efficiency. To optimize the efficiency of KI editing, the donor sequences were designed as single-

stranded oligo DNA nucleotides (ssODN), carrying the mutation of interest, and also included a silent (or blocking) mutation that mutates the protospacer-adjacent motif (PAM) or disrupts the sgRNA binding region to prevent re-cutting by Cas9 after successful editing[28,29,25,30]. The ssODN contained 100 nucleotides with homology arms on each side of the target region. The ssODN sequence was as follows (see also **Suppl. Tables S2 –S3)**:

For *TBX19*^{K146R} (5'-3'):

TGGATGAAAGCTCCCATCTCCTTCAGCAAAGTGAGGCTGACCAACAAGTTAAATGGAGGCGG GCAGGTACGAATGAGGCGGGCAGGCCTGGCCACCCGCT.

For *NFKB2*^{D865G} (5'-3'):

TCCCATTCCTGTCCCCATTTACCCCCAGCAGAGGTGAAGGAAGGCAGTGCCTACGGGAGCCAG TCAGTGGAGCAGGAGGCAGAGAAGCTGGGCCCACCCC.

The ssODN were synthesized by Integrated DNA Technologies (Coralville, Iowa, US) at Ultramer™ quality.

Electroporation

hiPSC were transfected with constructed sgRNA/Cas9 vectors by electroporation using the Neon Transfection System 100 µL kit (Invitrogen). A summary of the procedure is described in **Suppl. Figure S1**.

Clone isolation and screening

On day 3 post-transfection, we used a cleaved amplified polymorphic sequences (CAPS) assay to estimate the efficacy of CRISPR/Cas9 in bulk transfected hiPSC populations to choose the number of colonies to be picked[31]. A restriction enzyme recognition site is

inserted in the donor template. CAPS primers and restriction enzymes were determined with the help of AmplifX software (version 2.0.0b3; https://inp.univ-amu.fr/en/amplifx-manage-test-and-design-your-primers-for-pcr). CAPS primers were listed in **Suppl. Table S4**. The CAPS products were separated and visualized by electrophoresis on a 2% agarose gel and analyzed for densitometry with ImageJ[25,30].

After 10 days, the CAPS assay was also used to screen and identify the possible *knock-in* (KI) clones. KI clones were screened by CAPS assay and confirmed by Sanger sequencing (Genewiz, Leipzig, Germany). Analyses of Sanger traces were done by Sequencher DNA sequence analysis software (version 5.4.6, Gene Codes Corporation, Ann Arbor, MI USA, http://www.genecodes.com) to align sequences of KI clones with WT sequence to confirm the successful edition. Sanger sequencing primers are described in **Suppl. Table S4**. KI clones were kept, amplified and then cryopreserved.

In vitro pituitary organoids differentiated from hiPSC

Pituitary organoids were produced at the same time, using the same protocol for WT and edited hiPSC lines. Two batches of differentiation with two hundred organoids for each hiPSC line were generated:

Batch 1: WT organoids versus *TBX19* KI organoids

Batch 2: WT organoids versus *NFKB2* KI organoids

The differentiation protocol was based on a protocol from Matsumoto et al. with some modification.[20,22]. hiPSCs were first dissociated into single cells using Accutase. Ten thousand cells per organoid were plated in 20 µL hanging drop under the lid of a 127.8 x 85.5mm single-well plate (Greiner bio-one) in growth factor-free chemically defined

medium (gfCDM) supplemented with 10% (vol/vol) Knockout Serum Replacement (KSR; Thermo Fisher Scientific) and 20 μM Y-27632. The lid was inverted over the bottom chamber (filled with 10 mL of sterile water to avoid the evaporation of droplets) and incubated at 37°C/5% CO_2 for 2 days. Once aggregates formed, organoids were transferred to non-adhesive 100x20mm culture dishes (Corning) containing 10 mL of gfCDM medium supplemented with 10% KSR without Y-27632 and incubated at 37°C and 5% CO_2 until day 6. From days 6 to days 17, the medium was supplemented with 10% KSR, 5 nM recombinant human bone morphogenetic protein 4 (BMP4; Peprotech, # AF-120-05ET, USA) and 2 μM Smoothened agonist (SAG; Sigma-Aldrich/Merck, # SML 1314). Half of the medium was renewed every 2 - 3 days.

From day 18, BMP4 was withdrawn and half of the medium was renewed every 2 - 3 days. At this point, organoids were maintained under high-O_2 conditions (40%) and 5% CO_2 in an MCO-5M incubator (Panasonic). From day 30, gfCDM medium supplemented with 20% knockout serum replacement was used, and all medium was renewed every 2-3 days until at least day 105. Induction into pituitary progenitor cells (defined as LHX3+) and into pituitary hormone-producing cells was evaluated by qRT-PCR (on days 0, 6, 18, 27, 48, 75, 105) and immunofluorescence (on days 48 and 105) (see below).

Validating *TBX19*^{K146R} targeting and assessing off-target mutations by whole genome sequencing (WGS)

For *TBX19*^{K146R}, we used whole genome sequencing (WGS) to assess on-target and off-target mutations, because the edited site is far from the cut site (15 bases). DNA extracted from control and *TBX19* KI (5 organoids each) was submitted for WGS to an average depth of 15X (Integragen Genomics platform). PCR-free libraries were prepared

with the NEBNext Ultra™ II DNA Library Prep Kits (New England BioLabs) according to supplier recommendations. Specific double-strand gDNA quantification and a fragmentation (300 ng of input with high-molecular-weight gDNA) sonication method were used to obtain approximately 400 bp fragments. Finally, paired-end adaptor oligonucleotides (xGen TS-LT Adapter Duplexes from Integrated DNA Technologies) were ligated and re-paired. Tailed fragments were purified for direct sequencing without a PCR step. DNA PCR free libraries were sequenced on paired-end 150 bp runs on the NovaSeq6000 (Illumina) apparatus. Image analysis and base calling were performed using Illumina Real Time Analysis (RTA) Pipeline with default parameters. Sequence reads were mapped on the Human Genome Build (GRCh38) using the Burrows-Wheeler Aligner (BWA)[32]. Variant calling was performed via the GATK Haplotype Caller GVCF tool (GATK 3.8.1, Broad Institute)[33]. Mutation enrichment was determined using Fisher's Exact Test. Variants were annotated with Ensembl's Variant Effect Predictor, VEP) by Integragen Genomics[34]. NGS analyses confirmed the presence of on-target mutation and the absence of off-target mutation in the top four predicted off-target sites.

Validating *NFKB2^{D865G}* targeting, assessing off-target mutations and differential expression analysis by bulk RNA sequencing (RNA-seq)

For *NFKB2^{D865G}*, we used bulk RNA sequencing (RNA-seq) for analysis of differential RNA expression, and to assess on-target and off-target mutations, because the target site is close to the cleavage site (6 bases). A total of 500 ng of total RNA was extracted from 10 individual organoids (5 *NFKB2* KI and 5 control organoids). RNA-seq libraries were generated using the KAPA mRNA HyperPrep kit (Roche). The quality and profile of the libraries were visualized on a Bioanalyzer using the High Sensitivity DNA assay

(Agilent) and-quantified on a Qubit using the dsDNA High Sensibility Kit (Thermo Fisher Scientific). Finally, we performed a 2x 76-bp paired-end sequencing on a NextSeq500 (Illumina). After quality control using FastQC (Braham Institute), reads were aligned on the GRCh38 human reference genome using STAR (version 2.7.2b)[35]. BAM files were ordered and indexed using Samtools[36]. Read counts on genes were determined using StringTie[37]. We assessed the presence of desired *NFKB2* edits according to the CRISPR sgRNA design by direct visualization of the BAM files and the absence of off-target coding variations by the GATK Haplotype Caller GVCF tool [33]. Genes differentially expressed between conditions were identified using the R package DESeq2 (version 1.34.0)[38] and assigned as such with an adjusted P-value < 0.05.

Total RNA isolation and quantitative real-time PCR (qRT-PCR) analysis for assessment of mRNA expression during pituitary organoid development

Organoids were harvested from the culture, placed on ice and then stored at -80°C until RNA extraction. The total RNA was extracted from WT, *TBX19* KI and *NFKB2* KI organoids using the NucleoSpin RNA Plus XS kit (Macherey-Nagel), and measured on a NanoDrop TM 1000 Spectrophotometer (Thermo Fisher Scientific). Organoid RNAs were extracted on days 0, 6 and 18 from 7 or 8 organoids, or on days 27, 48, 75 and 105 from single organoids (3-8 organoids per group for each time point). cDNA was synthesized from 200 ng total RNA using the mix of M-MLV reverse transcriptase (Invitrogen, UK, #28025013), dNTP 10mM (Invitrogen, #10297018), RNAseOut Inhibitor (Invitrogen, #10777019) and random primers (Invitrogen, UK, #48190011). Quantitative PCR was performed using iTaq Universal SYBR Green Supermix (Bio-Rad

Laboratories), on Quantstudio™ 5 Real-time PCR system (Thermo Fisher Scientific) and analysed using QuantStudio™ 5 Design & Analysis Software. The thermal cycling profiles were as follows: initial denaturation at 95°C for 20 seconds, followed by 40 cycles of denaturation at 95°C (3 sec), annealing at 60°C (45 sec) and extension at 72°C (45 sec). All samples were assayed in duplicate. The beta-actin (*ACTB*), glyceraldehyde-3-phosphate dehydrogenase (*GAPDH*) and beta-tubulin (*TUBB)* transcripts expressions were used as three endogenous reference controls. Target gene expressions were normalized relative to the mean of the housekeeping genes using the delta Ct method. For gene expression kinetics, these values were normalized relative to the highest mean values of WT during 105 days using the comparative $2^{-\Delta\Delta Ct}$ method[39]. Primer sequences used in the experiments are shown in **Suppl. Table S7**.

Immunofluorescence labeling experiments

At days 48 and 105, ten of each WT and mutant organoids were fixed using 4% buffered paraformaldehyde in standard phosphate-buffered saline (PBS) for an hour at RT before rinsing in PBS. After overnight incubation in 30% sucrose/PBS (w/v) at 4°C, organoids were embedded in Surgipath medium (Leica) and snap frozen. Organoids were cryosectioned at 16 µm. After blocking with 0.01% Triton X100, 10% normal donkey serum, and 1% fish skin gelatin in PBS with 5 ng/mL 4',6-diamidino-2-phénylindole (DAPI) for an hour at RT, slides were incubated with primary antibody diluted in antibody solution (PBS, Triton as above, 1% normal donkey serum and 0.1% fish skin gelatin) overnight at 4°C, washed and incubated in a 1/500 dilution of secondary antibody in PBS for 2 hours at RT. The primary antibodies and dilutions used in this

study are summarized in **Suppl. Table S8**. Secondary antibodies were species-specific conjugates to Alexa Fluor 488, 555 or 647 (Thermo Fisher Scientific). Fluorescence images were obtained using LSM 800 confocal microscopy (Zeiss).

3D imaging of pituitary organoids

We used a whole-mount immunostaining and clearing protocol adapted from Belle et al [40]. 4-8 organoids of each genotype (WT, *TBX19* KI or *NFKB2* KI) were fixed by immersion in 4 % buffered paraformaldehyde (PFA) in PBS overnight at 4°C. All steps were carried out on a slowly rotating (70 rpm) agitator. After washing in PBS, organoids were either stored at 4°C or blocked and permeabilized with 5 mL PBSGT for 2 days at RT (PBSGT: 0.2% fish skin gelatin, 0.5% Triton X100 in PBS, NaN_3 0.01%). Organoids were incubated with primary antibodies in 3 mL PBSGT (at concentrations used on sections) over 5 days at 37°C to increase penetration. Organoids were then washed 6 times in an excess of PBSGT at RT, before incubation with secondary antibodies in 3ml PBSGT at RT overnight. The wash step was repeated. Organoids were then embedded in 1% low-melting temperature agarose in 1X TAE after it had cooled to about 45°C.

As adapted from the iDISCO+ protocol[41], organoids in agarose blocks were progressively dehydrated from 20%, 40%, 60%, and 80% to 100% methanol for 1h at each graded step. After overnight incubation in two parts dichloromethane (DCM, Sigma-Aldrich) to one part 100% methanol, organoids were immersed in 100% DCM for 30 minutes before changing to 100% dibenzyl ether (DBE; Sigma-Aldrich) for transparization over two hours. Samples were maintained in DBE at RT and protected from light in an amber glass vial. Light-sheet fluorescence microscopy (Miltenyi Biotec UltraMicroscope Blaze™) was used to acquire z-stacks of optical sections of pituitary

organoids at 4 µm intervals, in Ethyl cinnamate (Sigma-Aldrich). After 3D reconstruction with Imaris software (version 9.6, Bitplane), the number of corticotrophs in each organoid was defined by counting individualized cell-sized (7 µm) objects positive for ACTH immunoreactivity with the Spots automatic classifier after setting parameters in a region of interest containing positively labeled WT cells, then applied to all organoids. Using the Surfaces tool of the Imaris software, the volume of organoids was determined based on thresholds corresponding to their respective fluorescence intensities.

Statistical analysis

Statistical analyses were performed and visualized with GraphPad Prism 9.5.0 software (GraphPad Software, Inc). Data are expressed as means ± SEM. Comparisons between the two groups (mutant versus WT) were performed by unpaired two-tailed t-tests (non-parametric Mann-Whitney test). n refers to the number of samples for each experiment outlined in the figure legends. p values of < 0.05 (*), < 0.01 (**), and < 0.001 (***) were considered statistically significant differences.

Results

Corticotroph deficiency can be modeled by directed differentiation of *TBX19*-mutant hiPSC in 3D culture

To first validate the pituitary organoid model and determine whether the *TBX19* mutant can affect corticotrophs differentiation, we generated a *TBX19* KI hiPSC line from the control line using CRISPR/Cas9 (**Figures 1A-1D; Suppl. Figure S1**). One KI clone carrying $TBX19^{K146R/K146R}$ was obtained after screening 100 clones by CAPS and confirmation by Sanger sequencing (**Suppl Figure S2**). This mutant clone was then amplified and differentiated into pituitary organoids, in parallel with the control line.

The ability of the *TBX19* KI line to differentiate into the hypothalamo-pituitary structure was compared to the control line (200 organoids for each line) using a 3D organoid culture method, in which pituitary-like and hypothalamus-like structures simultaneously develop (**Figures 1E, 2A, Suppl Figure S3A-B**). In this method, hiPSC differentiate into hypothalamic progenitors in the central part of the organoids, whereas the outer layer differentiates into oral ectoderm, that will in turn develop into anterior pituitary tissue (**Figure 2A**, **Suppl Figure S3**). The expression of several key markers of pituitary development and differentiation was then compared in mutant *TBX19* KI organoids over time, matched to control WT organoids using qRT-PCR (d0, d6, d18, d27, d48, d75, d105) and immunofluorescence (d48 and d105) (**Figure 2A)**. Organoids grew in the culture medium with average sizes in their greatest dimension from 0.4 mm on day 6 to 1.9 mm on day 105 (**Figure 2B**).

Successful differentiation was validated in WT organoids by qRT-PCR, at early stages by the expression of a set of pituitary transcription factors, including *HESX1*, *PITX1* and

LHX3, and at the latest stage of corticotroph cell differentiation by the expression of *TBX19* and *POMC* (**Figures 2A, 2C-2H**). HESX1 is the first specific marker of pituitary primordium and its expression is important for the early determination of the gland. In WT organoids, *HESX1* peaked around day 6 of culture, and was rapidly downregulated from day 18 **(Figure 2D)**. Expression of *PITX1* (oral ectoderm marker) and *LHX3* (pituitary progenitor marker) increased from day 27, then *PITX1* reached a plateau from d48 **(Figure 2E)** whereas *LHX3* peaked at d75 and was then slightly downregulated **(Figure 2F)**. Immunofluorescence confirmed the presence of oral ectoderm cells expressing PITX1 and CDH1 (E-cadherin, **Suppl Figure S3C**), therefore resembling Rathke's pouch progenitors. The effective generation of pituitary progenitors was confirmed by the presence of LHX3+ cells in WT organoids on day 48 (**Figure 3A, Suppl Figure S3A**). These cells were located in the outermost layer of WT organoids, surrounding the hypothalamic progenitor layer that expressed NKX2.1 (**Suppl Figure S3B**). By day 105, WT organoids contained many differentiated corticotrophs co-expressing TBX19 protein in the nucleus and ACTH in the cytoplasm, as seen in confocal microscopy, a critical feature for the rest of our investigations (n=8, **Figure 3B, Suppl Figure S3D**). Consistent with these images, qRT-PCR results confirmed the highest levels of *TBX19* and *POMC* expression after at least 75 days of culture in WT organoids (**Figures 2G-2H**). Taken together, these data showed that pituitary organoids in 3D culture mimic human pituitary ontogenesis, and were characterized in our conditions by the ability to differentiate into pituitary progenitors by day 48 and into corticotroph cells by day 105.

We then tested whether ACTHD could be modeled by *TBX19*-mutant pituitary organoids. To this end, the development of pituitary organoids carrying *TBX19* KI was

matched to WT organoid development and analyzed using qRT-PCR and immunofluorescence for pituitary ontogenesis markers as described above. Our data showed a significant decrease in the expression of *HESX1* at d18 and d27 in the mutant (**Figure 2D**). Both *PITX1* and *LHX3* transcript levels were significantly decreased by day 48 and day 75 in mutant organoids (**Figure 2E and 2F**), with only partial recovery for *PITX1* by d105, suggesting an impairment of pituitary progenitor generation. Although *TBX19* transcript levels were unchanged until d75 (**Figure 2G**), we observed a decrease in *POMC* expression in the *TBX19* KI organoids that was significant from day 48 onwards (**Figure 2H**). *TBX19* expression was significantly higher in mutant organoids at d105, but this had no influence on *POMC* expression, which remained very low. These results confirmed that our organoid model can recapitulate the need for a fully functional TBX19 protein to achieve proper *POMC* gene transcription during human pituitary development.

Next, we checked several pituitary markers by immunofluorescence (**Figures 3A-3D**). In line with qRT-PCR results, *TBX19* KI organoid immunostaining on day 48 showed that LHX3 protein expression was decreased in *TBX19* KI organoids (n= 10 organoids for each group, **Figures 3A, 3B**). By day 105, we observed that there were significantly fewer corticotroph cells expressing ACTH and TBX19 proteins in $TBX19^{K146R/K146R}$ organoids (n= 10 organoids for each group, **Figures 3C, 3D**).

Finally, in order to take into account the possibility of regionalized sampling in the section, we performed quantitative analysis of ACTH by transparizing organoids immunostained for the hormone and imaging them by light-sheet confocal microscopy. 3D reconstruction confirmed that ACTH was nearly absent from *TBX19* KI organoids on day 105 compared to control organoids (**Figures 4A-4B** and **Suppl Movies 1-2**). We

observed that corticotroph cell distribution was not uniform throughout the organoids, but was rather concentrated in one or a few buds. In summary, there was a significant decrease in the number of ACTH+ corticotroph cells with a *TBX19* KI genotype on day 105 versus control organoids (**Figure 4C**).

Together, this first set of experiments demonstrated that genome editing of hiPSC with a KI homozygous pathogenic variant of *TBX19* effectively prevented their differentiation into ACTH-producing corticotrophs.

NFKB2 signaling is vital for corticotroph development

As our organoid model for the study of ACTHD was validated with the *TBX19* mutant line, we then used the same approach to investigate the potential role of NFKB2 in human hypothalamic-pituitary development. To do so, we first established a *NFKB2* KI mutant hiPSC line using CRISPR/Cas9 (**Figure 5**) from an isogenic control. The $NFKB2^{D865G}$ homozygous mutation was chosen because it has been shown to severely affect NFKB2 p52 processing[12]. Two homozygous KI clones carrying $NFKB2^{D865G/D865G}$ were obtained after screening by CAPS and confirmation by Sanger sequencing (**Suppl Figure S4**). We selected one homozygous missense mutation *NFKB2* KI clone (#7) to amplify and generated 200 mutant organoids in parallel with 200 WT organoids in 3D culture.

Next, we compared the development and differentiation of the *NFKB2* KI organoids versus WT organoids during the culture by qRT-PCR and immunofluorescence as described above. The results of qRT-PCR showed no significant difference in the peak expression level of *HESX1.* However, higher *HESX1* expression in mutant organoids from

d27 to d75 suggested impaired downregulation of the gene (**Figure 6B**). Concomitantly, a significantly decreased expression of *PITX1* and *LHX3* in *NFKB2* KI organoids was found from d48 onwards, suggesting reduced differentiation of pituitary progenitors (**Figures 6C-6D**). Similar to what we observed in *TBX19* KI mutants, *TBX19* expression was increased in *NFKB2* KI organoids at d105 (**Figure 6E**). However, this had no impact on *POMC* expression levels, which remained significantly lower in *NFKB2 KI* organoids (**Figure 6F**), suggesting a role for NFKB2 in corticotroph terminal differentiation.

As MRI had revealed pituitary hypoplasia in 43% of patients with DAVID syndrome[42], we investigated whether mutant organoids might be smaller than WT organoids. Comparing the volume of both types of organoids on day 105, we found no significant difference (p= 0.6, WT n=7, mutant n= 8, **Figure 6G**). In line with qRT-PCR results, immunostaining showed less expression of LHX3 in *NFKB2* KI organoids on day 48 compared to the WT (**Figures 7A-7B**). NFKB2 (the antibody did not discriminate between p100/p52 isoforms) was robustly expressed in WT LHX3+ pituitary progenitors on day 48 (**Figure 7A**). Unexpectedly, NFKB2 p100/p52 immunostaining was weaker in *NFKB2* KI organoids than in WT organoids (**Figures 7A-7B**). Immunostaining at d105 in *NFKB2* KI organoids showed the presence of many TBX19+ nuclei, in line with the qRT-PCR results, but few of them were surrounded by cytoplasmic ACTH signal (**Figures 7C-7D)**. Quantification after 3D reconstruction of transparent whole organoids showed significantly fewer ACTH+ cells in *NFKB2* KI organoids on day 105 compared to WT organoids in both qualitative (**Figures 8A-8B** and **Suppl Videos 3-4**) and quantitative (**Figure 8C**) assessments. In the absence of an immune system, this is strong evidence in support of a direct role for NFKB2 signaling in pituitary differentiation.

To further investigate other downstream pathways altered in *NFKB2* KI pituitary organoids, we performed whole RNA-seq of five distinct organoids on day 48 from the *NFKB2* KI line versus five organoids derived from its corresponding hiPSC control line. As we found that only 60-70% of organoids show signs of pituitary cell differentiation, we chose to perform a preselection of organoids, based on RT-qPCR expression of selected markers (*SOX2*, *HESX1*, *PITX1*, *LHX3*, *TBX19*, *POU1F1* and *POMC*) in order to avoid having "empty" HPOs sent for bulk RNAseq. Differential expression (DE) gene analysis identified 2559 significantly upregulated and 2260 significantly downregulated genes at adjusted p value (pAdj) < 0.05. The global results are depicted as a heatmap to show the similarities across organoids of similar genotypes (**Figure 9A**) and a volcano plot highlights the magnitudes of DE between the two groups (**Figure 9B**).

NFKB signaling did not seem to be affected in *NFKB2* KI organoids, as most genes involved in that pathway had fold-change values between -0.5 and 0.5 when significant (**Suppl Figure S5**). Among a list of 144 genes known to have a functional influence on pituitary-hypothalamic development as curated from the published literature, 67 were found to be differentially expressed in *NFKB2* KI organoids (pAdj < 0.05) (**Figure 9B**, and **Table 1**), of which 39 encode transcription factors (**Figure 9C**). Expression of these transcription factors was mostly downregulated, with a marked decrease in expression of pituitary progenitor markers such as *PITX1* and *LHX3*. In contrast, the earliest Rathke's pouch marker, *HESX1,* showed a 2-fold increased expression in *NFKB2* KI organoids, suggesting impaired progression of pituitary progenitors towards more differentiated stages.

During pituitary development, progenitors undergo epithelial to mesenchymal transition (EMT). Data from human fetuses[16] suggest that pituitary stem

cells/progenitors are in an hybrid state, as they simultaneously express "stemness" as well as epithelial and mesenchymal-associated genes, and expression of all these gene sets decrease in concert during the course of differentiation. While the overall number of anterior pituitary-type cells in *NFKB2* KI organoids was not affected, as confirmed by RT-qPCR of the pan-pituitary cell adhesion marker *EPCAM*, there was a significant decrease in the expression of stemness markers such as *HES1*, *SOX2* and *SOX9* **(Table 2, left panel)**, accompanied by increased expression of stem cell-associated epithelial markers *CDH1* and *KRT8* **(Table 2, middle panel)** and decreased expression of stem cell-associated mesenchymal markers *CDH2* and *VIM*. Other mesenchymal markers expressed in both stem cells and differentiating cells (*COL1A1* and *COL1A2*) were upregulated **(Table 2, right panel)**. *CLDN6*, which is expressed in early pituitary progenitors[16], was upregulated (fold change = 2.3; $p<0.0001$) whereas *CLDN9*, widely expressed in the fetal human pituitary[16], was decreased (fold change = 0.34; $p<0.0001$). Overall, these results suggest that progenitors initiate EMT, but stall during the process. Of note, the expression of *ZEB2*, *SNAI1* and *SNAI2*, key initiators of EMT through the downregulation of *CDH1*, is significantly increased (fold changes of 1.37, 3.37, and 5.36, respectively; $p< 0.01$), suggesting that *NFKB2* plays an important role downstream from these effectors.

TBX19 KI and *NFKB2* KI alter hypothalamic-pituitary organoid development through distinct mechanisms

The transcription factor *RAX,* which is physiologically expressed in the hypothalamus, also showed a moderate but significant decrease in its expression in *NFKB2* KI organoids (**Figure 9C** and **Table 1)**, suggesting that the phenotype could at least partially be due to a hypothalamic defect. Indeed, among the growth factors known to

mediate the interaction between hypothalamus and oral ectoderm during pituitary development in animal models, *BMP4, FGF8* and *FGF10* had fold-changes of 4.35, 0.5 and 0.26 in *NFKB2* KI organoids respectively, whereas *SHH*, *WNT5A* and *FGF8* expression levels were not modified (**Table 1**).

In comparing the results of RT-qPCR to those obtained by RNAseq, we found good correlations (R^2=0.7595; p<0.0001) between the *NFKB2* KI to WT ratios measured with both techniques on the same samples, except for *TBX19* (**Suppl Figure S7**). As we obtained similar results with 2 sets of *TBX19* RT-qPCR primers, targeting different exons, and with at least one primer hybridizing over the junction of two exons, we believe the RNAseq results for this gene to be likely biased, though we have not identified the reason.

Comparing gene expression levels between *TBX19* KI and *NFKB2* KI organoids of developmentally important transcription and growth factors shows their differences. As mentioned before, *HESX1* was downregulated at d48 only in *NFKB2* KI organoids, whereas both mutants had decreased levels of *PITX1* and *LHX3*, the latter being more severely impacted in *NFKB2* KI organoids (**Figure 10A**). In these, we confirmed the increase in *BMP4* and decrease in *FGF8*/*FGF10* expression seen in RNAseq. We did not find any significant differences in these transcripts between WT and *TBX19* KI organoids (**Figure 10B**), suggesting that the impaired development of pituitary progenitors in this model has a different mechanism.

We then explored markers of different stages of corticotroph maturation that were recently identified in human fetal pituitary[16]. RNAseq on d48 *NFKB2* KI organoids showed increased expression of *FST*, a gene expressed in immature corticotropes, and

concomitant decreased levels of fully mature corticotrope markers *AR*, *NR4A2*, *PCSK1* and *POMC* (0.63, 0.4, 0.35 and 0.43-fold changes respectively) (**Table 1)**. RT-qPCR at d48, d75 and d105 showed that *TBX19* was upregulated at later stages in both models, suggesting that both *TBX19* and p52 are involved in the control of *TBX19* expression (**Figure 11A**). The *NR4A2* transcription factor was downregulated at d75 in both mutants, but strongly upregulated in *TBX19* KI organoids and downregulated in *NFKB2* KI organoids at d105 (**Figure 11B**). *PCSK1* expression, necessary for prohormone processing, also decreased in both mutants, but this phenomenon started earlier in *NFKB2* KI organoids (**Figure 11C**). Finally, we found that *POMC* expression was as strongly impaired in *NFKB2* KI organoids as in *TBX19* KI organoids. These results, combined with normal expression levels for *NEUROD1*, corroborate the hypothesis that TBX19-positive precursors fail to achieve terminal differentiation in *NFKB2* KI organoids.

Interestingly, other lineages also appeared to be affected, both in *TBX19* KI and *NFKB2* KI organoids. RNA-seq at d48 showed drastic downregulation of *PROP1* and *POU1F1* transcription factors in *NFKB2* mutants. Although we could not accurately measure *POU1F1* expression at d48 due to its too low expression, RT-qPCR (**Figure 11**) showed that *PROP1* downregulation was also occurring in *TBX19* KI organoids at d48 (**Figure 11A, left**), and both *PROP1* and *POU1F1* levels were barely detectable at d75 in the two models (**Figure 11A and 11D**). This is likely to be the consequence of the impaired generation of pituitary progenitors described above. Nonetheless, other transcription factor markers of *POU1F1*-dependent lineages were expressed, as shown by normal expression of *NEUROD4* and *ZBTB20* in *TBX19* KI organoids at d48 (**Figure 11B and 11C, left**). However, both genes had lower expression levels at 75 compared to WT

(**Figure 11B and 11C, right**). In *NFKB2* KI organoids, *NEUROD4* was downregulated at both time points (**Figure 11B)**, and *ZBTB20* at d48 only (**Figure 11C, left**), with signs of recovery at d75 (**Figure 11C, right**) and d105 (data not shown). Again, these results suggest that different mechanisms converge on impaired POU1F1-dependent lineage development.

Finally, the glycoprotein hormone common alpha subunit *CGA* was strongly upregulated at d48 **(Table 1)** and d75 (data not shown) in *NFKB2* KI organoids. The concomitant increase in *GATA2*, *CYP11A1* and *FOLR1* may suggest a redirection of some progenitors towards a gonadotroph/thyrotroph cell fate. However, lack of changes in expression of *NR5A1*, *NEUROD1* and *SOX11*, and the undetectable transcripts for the specific beta subunits *FSHB*, *LHB* and *TSHB* before d105, do not favour this hypothesis.

A few years ago, ChIP-seq experiments on Hodgkin lymphoma cells[43] identified 10,893 DNA-binding regions for NFKB2 p52, within or in the close vicinity of 5,497 genes. About half of p52 recruitments occurred in transcribed regions, with a high percentage within introns, and the other half in intergenic regions close to a transcriptional start site (TSS). Among the 4,819 differentially regulated genes identified in *NFKB2* KI organoids at d48, 1,398 of them had p52 binding regions nearby **(Figure 12),** of which 23 belong to our curated list of pituitary genes of interest. Among them, we found genes crucial for progenitor development (*SOX9*, *PITX1*), EMT (*CDH1*, *ZEB2*), POU1F1-dependent lineages (*PROP1*, *NEUROD4*), and most importantly, the principal genes of corticotroph development and maturation (*TBX19*, *NR4A2*, *PCSK1*, *POMC*). Thus, these changes in the expression of these genes we observed in *NFKB2* KI organoids may be due to a direct effect on transcriptional regulation.

Altogether, our data identify the NFKB2 signaling pathway as an important factor acting at multiple levels on human pituitary development.

Discussion

After the description of DAVID syndrome as a rare combination of anterior pituitary deficit, mostly ACTHD, with common variable immunodeficiency, we and others found that it is associated with *NFKB2* gene mutations affecting specific C-terminal residues of the NFKB2 protein, known to play important roles in immunity and also expressed in the pituitary[7,8,9]. As the mouse model harboring a similar alteration of the ortholog gene lacked an endocrine phenotype[9], we wanted to investigate the mechanism of ACTHD in this syndrome. Currently available *in vitro* models to study ACTHD and CPHD have strong limits. For instance, studies based on transfections and luciferase-coupled hormone promoters can only give indirect evidence of the effect of a variant of unknown significance as they are based on partly arbitrary amounts of DNA and promoters in an artificial context[5]. Murine models only partially replicate human CPHD, as shown for *PROP1* mutations and the occurrence of ACTHD (absent in mice but present in 40% of humans)[44]. In the past decade, the reprogramming of differentiated adult cells into induced pluripotent stem cells and advancements in genome editing technologies using CRISPR/Cas9 systems have broadened possibilities for modeling novel aspects of human disease *ex vivo*[45]. Organoid culture has become a powerful tool for modeling otherwise inaccessible congenital human disorders in many organs such as brain[25], intestine[46], kidney[47], liver[48], pancreas[49], ovary[50], and lung[51]. In the present study, we established a human *in vitro* model of congenital ACTHD using 3D pituitary

organoids differentiated from *TBX19* KI and *NFKB2* KI hiPSC generated by CRISPR/Cas9 genome editing, in order to compare them with their WT equivalents on the same genetic background. After confirming that our model could replicate pituitary development, we then determined whether it could also replicate a disease, namely ACTHD. As the *TBX19*^{K146R} homozygous variant led to ACTHD in humans, we designed a human "KI" organoid model derived from *TBX19*$^{K146R/K146R}$ hiPSC. In line with the *Tbx19*$^{-/-}$ mouse model[3], *TBX19* KI organoids displayed markedly defective corticotroph differentiation, as compared to WT organoids, thereby validating the methodological approach. Interestingly, in organoids carrying a *TBX19*$^{K146R/K146R}$ missense mutation that affects DNA binding, a few corticotrophs were still present, suggesting either a role for TBX19 independent of its DNA binding activity or persistence of residual DNA binding activity with this mutation. This model also raises the possibility for a previously undescribed role of TBX19 during early development and the generation of pituitary progenitors in human. However, as *TBX19* mutations have only rarely been associated with other pituitary deficits - especially transient GHD[52], further investigations will be needed.

Using this same approach with *NFKB2*$^{D865G/D865G}$ human organoids generated by CRISPR/Cas9 genome edited hiPSC, we demonstrated for the first time a role for NFKB2 in pituitary development. Heterozygous mutations in the C-terminal region of *NFKB2*, such as D865G, were reported in DAVID syndrome, leading to the disruption of both non-canonical and canonical pathways[8,11–13,53,54]. Even though *NFKB2*^{D865G} was identified in a heterozygous state in patients with ACTHD, we decided to use a homozygous model of *NFKB2* KI to determine whether NFKB2 was involved in pituitary development and could explain the defect in ACTH production in DAVID syndrome

(OMIM#, 615577) [7,8,55]. Indeed, while concomitant common variable immune deficiency (CVID) can be explained by the key roles of NFKB signaling in the immune system, the mechanism of the endocrine deficits caused by *NFKB2* mutants was unknown. In mouse models, deletion of *Nfkb2* cause abnormal germinal center B-cell formation and differentiation[14]. However, the *Lym1* mouse model, which carries a truncating variant Y868* in the *Nfkb2* orthologue that prevents its cleavage into a transcriptionally active form, had apparently normal corticotroph function and ACTH expression in the pituitary in both heterozygotes and homozygotes[9], despite reduced fertility and more severe immune abnormalities in mutant *NFKB2* homozygotes[56]. Using pituitary organoids differentiated from a *NFKB2* KI hiPSC line in comparison with its unmutated control and in the absence of an immune response, we have demonstrated that human corticotroph development is directly disrupted by the missense mutation found in DAVID syndrome. The absence of global alteration of NFKB signaling pathway shows that mutant p100/p52 protein is directly responsible for the observed phenotype.

The precise molecular mechanisms by which *NFKB2* mutation impairs corticotroph development remain to be determined. However, our results (summarized in **Figure 14**) suggest both early effects on the maturation of pituitary progenitors, on epithelial to mesenchymal transition, and late effects on corticotroph differentiation. First, The *NFKB2* gene product p52 could be involved in the early steps of pituitary development. RNA-seq data on day 48 of *NFKB2* KI organoid development showed increased *HESX1* and *BMP4* transcription, in favor of a blockade in an undifferentiated state evocative of the Rathke's pouch epithelial primordium: indeed, down-regulation of HESX1 is necessary for proper pituitary development[57]. This is also suggested by RNA-seq results showing downregulation of *PITX1, HES1, LHX3* and *FGF10* in mutant organoids, whereas

their expression is necessary for progression to a progenitor state[58,59]. The shift in the *BMP4/FGF10* balance favors the idea that the impaired differentiation of pituitary progenitors is at least in part of hypothalamic origin. Our results also suggest a disorganized EMT process, and the need for a functional p100/p52 to mediate the action of EMT inducers on CDH1 downregulation. Finally, concordant with the hypothesis of a differentiation blockade, upregulation of epithelial markers such as *CDH1* and *KRT8* was observed in mutant *NFKB2* KI organoids on day 48. In contrast, RNA-seq showed no change in Wnt and Hedgehog signaling pathways in *NFKB2* KI organoids.

The *NFKB2* gene product p52 could also be involved in the final steps of corticotroph differentiation. While qRT-PCR showed increased levels of *TBX19* mRNA in mutant organoids, this did not lead to the expected increase in *POMC* mRNA transcripts. Moreover, some *NFKB2* mutants had TBX19+ cells without ACTH expression. This suggests that p52 is necessary for POMC synthesis, which $NFKB2^{D865G}$ may prevent. This could be due to an abnormal DNA binding of the NFKB heterodimer to the *POMC* promoter[60,61], but as other NFKB binding sites are found in intronic regions, it may also be involved in changes in chromatin structures required for proper transcription. The same possibilities apply to *PCSK1*, the gene coding for the enzyme necessary for POMC to ACTH conversion, and to other genes involved in corticotroph maturation. Besides, $NFKB2^{D865G}$ could also block TBX19+ cells in a pre-differentiated state of corticotroph cells expressing FST through its derepression of chromatin remodeling factors such as EZH2[62].

GH deficiency has been reported in some patients with heterozygous *NFKB2* mutations[15]. The drastic effect on *POU1F1* expression we observed is likely to be the

consequence of different phenomena. First, the impaired development of progenitors, and the disruption of *PROP1* expression, possibly due to the absence of p52. Second, both *FOXO1* and *NEUROD4* have p52 binding regions and were differentially expressed. Alongside *POU1F1*, these two genes have been described as crucial members of a feedforward loop controlling somatotroph function[63]. The 12-fold increase in *CGA* expression and increased expression of pre-gonadotropes or mature thyrotropes (*GATA2*) and mature gonadotropes (*GATA2, CYP11A1* and *FOLR1*) could be an argument in favor of a redirection of pituitary progenitors towards these lineages. However, lack of differential expression of *NR5A1* contradicts this hypothesis. A more likely explanation is that *CGA* repression by TBX19 may directly require p52.

The organoid model described in this article presents several advantages over other approaches. It is a true human model of ACTHD, emphasizing the limits of mouse models, as exemplified by the *Lym1* model, which showed that *Nfkb2* p100/p52 function was not essential for pituitary development in mice, but did not provide insights for humans. *Nfkb2*$^{Lym1/Lym1}$ mice and our *NFKB2* KI model have different but functionally very similar mutations, as they both lead to an abnormal processing of p100 with its accumulation leading to a strong reduction of p52 content. The phenotype of *Nfkb2*$^{Lym1/Lym1}$ being more severe than in mice lacking the complete NFKB2 protein (*Nfkb2*$^{-/-}$), these dominant-negative mutations have been called "super repressors"[56]. In light of our results, it is surprising that no pituitary deficiencies have been observed in *Nfkb2*$^{-/-}$ or *Nfkb2*$^{Lym1/Lym1}$. This suggests that in human, *NFKB2* plays an important role during pituitary development, therefore constituting a major inter-species difference. Studying p52 binding regions across different species may help understand how this role appeared during evolution.

All patients with DAVID syndrome harbour heterozygous *NFKB2* mutations. Whether this reflects embryonic lethality of the mutation at the homozygous state or just the rarity of this genotype is still an unresolved question. However "super repressor" mutations have been shown to disturb both canonical and non-canonical signalling pathways even when heterozygous[10,11]. As our results show impaired POU1F1-dependent lineages development in addition to the severe corticotroph deficit, further experiments on organoids derived from *NFKB2*$^{WT/D865G}$ hiPSCs should tell if there are differences in the sensitivity of different lineages to the dominant-negative protein. If so, this could give us clues about why DAVID patients suffer from isolated ACTHD in their vast majority rather than CPHD.

Despite some technical limits, CRISPR/Cas9-based genome editing of hiPSC is a powerful approach to elucidate gene function in congenital pituitary deficiency patients, as was shown for the role of hypothalamic OTX2 regulation of pituitary progenitor cells in congenital pituitary hypoplasia[20]. While the prevalence of pathogenic variants of known genes in primary hypopituitarism is currently estimated at below 10%[6], exome and whole-genome sequencing regularly identify new genes and variants, for which pathogenicity remains uncertain[35]. This model could thus become in the following years the gold standard to confirm the involvement of a given gene in pituitary development, or to classify new variants of unknown significance as likely benign or pathogenic. Finally, pituitary organoids derived from human embryonic stem cells have been transplanted subcutaneously into mice with hypopituitarism; grafted cells were able to secrete ACTH and respond to corticotropin-releasing hormone stimulation[64], paving the way for innovative substitutive treatments in patients with hypopituitarism[65]. Conversely, a limitation of this model is the long duration of the differentiation period

(approximately 3 months) and the fact that not all hiPSC clones lead to full differentiation of hypothalamo-pituitary organoids despite similar conditions of culture. For these reasons, we could not include confirmation of our results on an independent clone in the present paper.

In conclusion, we have designed and validated a model replicating human constitutive ACTHD using a combination of CRISPR/Cas9 and directed differentiation of hiPSC into 3D hypothalamic-pituitary organoids. Not only has this proof-of-concept reproduced the known prerequisite for the TBX19 transcription factor in human corticotroph differentiation, but it has also allowed a new classification of a *NFKB2* variant of previously unknown clinical significance as pathogenic in pituitary development.

From a clinical viewpoint, this organoid model could provide evidence for the pathogenic role of new candidate genes or variants investigated in patients where none other is available, especially in a rare disease affecting a poorly accessible organ like the pituitary gland. From a physiological viewpoint, modeling corticotroph deficiency using hiPSC allows us to find evidence for a functional role for *NFKB2* in human pituitary differentiation.

Future studies investigating the direct role of p52 on transcription and changes in chromatin landscape during pituitary development will be necessary to elucidate its precise mechanism of action, as well as the level of pathogenicity of the $NFKB2^{D865G}$ mutations in its heterozygous form.

Acknowledgments

This study was supported by the ADEREM (Association pour le Développement de la Recherche Médicale au CHU de Marseille), the AFM-Telethon MoThARD grant to TB, and by Pfizer. TTM received funding from France Excellence Scholarship of the French Embassy in Vietnam, from the French Society of Pediatric Endocrinology and Diabetology (SFEDP) and from the Marseille Rare Disease (MarMaRa) Institute of Aix-Marseille University. The authors wish to thank Frederique Magdinier, Natacha Broucqsault and Claire El Yazidi from the Marseille Medical Genetics (MMG) cell reprogramming & differentiation facility (MaSC); Sébastien Courrier, from the MMG microscopy platform; Valerie Delague, Catherine Aubert, Christel Castro and Camille Humbert from MMG's Genomics and Bioinformatics (GBiM) platform; Carole Siret and Mathieu Fallet from the Centre d'Immunologie de Marseille-Luminy (CIML); Ivo Vanzetta and Alberto Lombardini from the Institut de Neurosciences de la Timone (INT) microscopy platform, and Laurie Arnaud and Emmanuel Nivet from the Institut de Neurophysiopathologie (INP), all in Marseille, for their expert assistance, advice or reagents.

Declaration of interests

The authors declare no competing interests.

References

1. Couture C, Saveanu A, Barlier A, et al. Phenotypic Homogeneity and Genotypic Variability in a Large Series of Congenital Isolated ACTH-Deficiency Patients with *TPIT* Gene Mutations. *The Journal of Clinical Endocrinology & Metabolism*. 2012;97(3):E486-E495. doi:10.1210/jc.2011-1659

2. Lamolet B, Pulichino AM, Lamonerie T, et al. A Pituitary Cell-Restricted T Box Factor, Tpit, Activates POMC Transcription in Cooperation with Pitx Homeoproteins. *Cell*. 2001;104(6):849-859. doi:10.1016/S0092-8674(01)00282-3

3. Pulichino AM, Vallette-Kasic S, Couture C, et al. Human and mouse *TPIT* gene mutations cause early onset pituitary ACTH deficiency. *Genes Dev*. 2003;17(6):711-716. doi:10.1101/gad.1065603

4. Reynaud R, Gueydan M, Saveanu A, et al. Genetic screening of combined pituitary hormone deficiency: experience in 195 patients. *J Clin Endocrinol Metab*. 2006;91(9):3329-3336. doi:10.1210/jc.2005-2173

5. Jullien N, Romanet P, Philippon M, et al. Heterozygous LHX3 mutations may lead to a mild phenotype of combined pituitary hormone deficiency. *Eur J Hum Genet*. 2019;27(2):216-225. doi:10.1038/s41431-018-0264-6

6. Jullien N, Saveanu A, Vergier J, et al. Clinical lessons learned in constitutional hypopituitarism from two decades of experience in a large international cohort. *Clin Endocrinol (Oxf)*. 2021;94(2):277-289. doi:10.1111/cen.14355

7. Quentien MH, Delemer B, Papadimitriou DT, et al. Deficit in Anterior Pituitary Function and Variable Immune Deficiency (DAVID) in Children Presenting with Adrenocorticotropin Deficiency and Severe Infections. *The Journal of Clinical Endocrinology & Metabolism*. 2012;97(1):E121-E128. doi:10.1210/jc.2011-0407

8. Chen K, Coonrod EM, Kumánovics A, et al. Germline Mutations in NFKB2 Implicate the Noncanonical NF-κB Pathway in the Pathogenesis of Common Variable Immunodeficiency. *The American Journal of Human Genetics*. 2013;93(5):812-824. doi:10.1016/j.ajhg.2013.09.009

9. Brue T, Quentien MH, Khetchoumian K, et al. Mutations in NFKB2 and potential genetic heterogeneity in patients with DAVID syndrome, having variable endocrine and immune deficiencies. *BMC Med Genet*. 2014;15:139. doi:10.1186/s12881-014-0139-9

10. Wirasinha RC, Davies AR, Srivastava M, et al. *Nfkb2* variants reveal a p100-degradation threshold that defines autoimmune susceptibility. *Journal of Experimental Medicine*. 2021;218(2):e20200476. doi:10.1084/jem.20200476

11. Kuehn HS, Niemela JE, Sreedhara K, et al. Novel nonsense gain-of-function NFKB2 mutations associated with a combined immunodeficiency phenotype. *Blood*. 2017;130(13):1553-1564. doi:10.1182/blood-2017-05-782177

12. Lee CE, Fulcher DA, Whittle B, et al. Autosomal-dominant B-cell deficiency with alopecia due to a mutation in NFKB2 that results in nonprocessable p100. *Blood*. 2014;124(19):2964-2972. doi:10.1182/blood-2014-06-578542

13. Lindsley AW, Qian Y, Valencia CA, Shah K, Zhang K, Assa'ad A. Combined immune deficiency in a patient with a novel NFKB2 mutation. *J Clin Immunol*. 2014;34(8):910-915. doi:10.1007/s10875-014-0095-3

14. Carragher D, Johal R, Button A, et al. A Stroma-Derived Defect in NF-κB2−/− Mice Causes Impaired Lymph Node Development and Lymphocyte Recruitment. *The Journal of Immunology*. 2004;173(4):2271-2279. doi:10.4049/jimmunol.173.4.2271

15. Mac TT, Castinetti F, Bar C, et al. Deficient anterior pituitary with common variable immune deficiency (DAVID syndrome): a new case and literature reports. *J Neuroendocrinol*. Published online May 6, 2023:e13287. doi:10.1111/jne.13287

16. Zhang S, Cui Y, Ma X, et al. Single-cell transcriptomics identifies divergent developmental lineage trajectories during human pituitary development. *Nat Commun*. 2020;11(1):5275. doi:10.1038/s41467-020-19012-4

17. Ho BX, Pek NMQ, Soh BS. Disease Modeling Using 3D Organoids Derived from Human Induced Pluripotent Stem Cells. *Int J Mol Sci*. 2018;19(4):E936. doi:10.3390/ijms19040936

18. Ozone C, Suga H, Eiraku M, et al. Functional anterior pituitary generated in self-organizing culture of human embryonic stem cells. *Nat Commun*. 2016;7(1):10351. doi:10.1038/ncomms10351

19. Kasai T, Suga H, Sakakibara M, et al. Hypothalamic Contribution to Pituitary Functions Is Recapitulated In Vitro Using 3D-Cultured Human iPS Cells. *Cell Reports*. 2020;30(1):18-24.e5. doi:10.1016/j.celrep.2019.12.009

20. Matsumoto R, Suga H, Aoi T, et al. Congenital pituitary hypoplasia model demonstrates hypothalamic OTX2 regulation of pituitary progenitor cells. *Journal of Clinical Investigation*. 2019;130(2):641-654. doi:10.1172/JCI127378

21. Suga H, Kadoshima T, Minaguchi M, et al. Self-formation of functional adenohypophysis in three-dimensional culture. *Nature*. 2011;480(7375):57-62. doi:10.1038/nature10637

22. Sasai Y, Eiraku M, Suga H. In vitro organogenesis in three dimensions: self-organising stem cells. *Development*. 2012;139(22):4111-4121. doi:10.1242/dev.079590

23. Sun Y, Ding Q. Genome engineering of stem cell organoids for disease modeling. *Protein Cell*. 2017;8(5):315-327. doi:10.1007/s13238-016-0368-0

24. Giobbe GG, Michielin F, Luni C, et al. Functional differentiation of human pluripotent stem cells on a chip. *Nat Methods*. 2015;12(7):637-640. doi:10.1038/nmeth.3411

25. Arnaud L, Benech P, Greetham L, et al. APOE4 drives inflammation in human astrocytes via TAGLN3 repression and NF-κB activation. *Cell Rep*. 2022;40(7):111200. doi:10.1016/j.celrep.2022.111200

26. Ran FA, Hsu PD, Wright J, Agarwala V, Scott DA, Zhang F. Genome engineering using the CRISPR-Cas9 system. *Nat Protoc*. 2013;8(11):2281-2308. doi:10.1038/nprot.2013.143

27. Concordet JP, Haeussler M. CRISPOR: intuitive guide selection for CRISPR/Cas9 genome editing experiments and screens. *Nucleic Acids Res*. 2018;46(Web Server issue):W242-W245. doi:10.1093/nar/gky354

28. Paquet D, Kwart D, Chen A, et al. Efficient introduction of specific homozygous and heterozygous mutations using CRISPR/Cas9. *Nature*. 2016;533(7601):125-129. doi:10.1038/nature17664

29. Edmondson C, Zhou Q, Liu X. Analysis of conventional and alternative CRISPR/Cas9 genome editing to enhance a single-base pair knock-in mutation. *BMC Biotechnology*. 2021;21(1):45. doi:10.1186/s12896-021-00707-5

30. Kwart D, Paquet D, Teo S, Tessier-Lavigne M. Precise and efficient scarless genome editing in stem cells using CORRECT. *Nat Protoc*. 2017;12(2):329-354. doi:10.1038/nprot.2016.171

31. Zischewski J, Fischer R, Bortesi L. Detection of on-target and off-target mutations generated by CRISPR/Cas9 and other sequence-specific nucleases. *Biotechnology Advances*. 2017;35(1):95-104. doi:10.1016/j.biotechadv.2016.12.003

32. Li H, Durbin R. Fast and accurate short read alignment with Burrows–Wheeler transform. *Bioinformatics*. 2009;25(14):1754-1760. doi:10.1093/bioinformatics/btp324

33. Poplin R, Ruano-Rubio V, DePristo MA, et al. Scaling accurate genetic variant discovery to tens of thousands of samples. Published online July 24, 2018:201178. doi:10.1101/201178

34. McLaren W, Gil L, Hunt SE, et al. The Ensembl Variant Effect Predictor. *Genome Biology*. 2016;17(1):122. doi:10.1186/s13059-016-0974-4

35. Dobin A, Davis CA, Schlesinger F, et al. STAR: ultrafast universal RNA-seq aligner. *Bioinformatics*. 2013;29(1):15-21. doi:10.1093/bioinformatics/bts635

36. Danecek P, Bonfield JK, Liddle J, et al. Twelve years of SAMtools and BCFtools. *GigaScience*. 2021;10(2):giab008. doi:10.1093/gigascience/giab008

37. Pertea M, Pertea GM, Antonescu CM, Chang TC, Mendell JT, Salzberg SL. StringTie enables improved reconstruction of a transcriptome from RNA-seq reads. *Nat Biotechnol*. 2015;33(3):290-295. doi:10.1038/nbt.3122

38. Love MI, Huber W, Anders S. Moderated estimation of fold change and dispersion for RNA-seq data with DESeq2. *Genome Biology*. 2014;15(12):550. doi:10.1186/s13059-014-0550-8

39. Livak KJ, Schmittgen TD. Analysis of relative gene expression data using real-time quantitative PCR and the 2(-Delta Delta C(T)) Method. *Methods*. 2001;25(4):402-408. doi:10.1006/meth.2001.1262

40. Belle M, Godefroy D, Couly G, et al. Tridimensional Visualization and Analysis of Early Human Development. *Cell*. 2017;169(1):161-173.e12. doi:10.1016/j.cell.2017.03.008

41. Renier N, Adams EL, Kirst C, et al. Mapping of brain activity by automated volume analysis of immediate early genes. *Cell*. 2016;165(7):1789-1802. doi:10.1016/j.cell.2016.05.007

42. Mac TT, Castinetti F, Bar C, et al. Anterior pituitary hormone deficiency in DAVID syndrome. *Journal of Neuroendocrinology*. n/a(n/a):e13287. doi:10.1111/jne.13287

43. Oliveira KAP de, Kaergel E, Heinig M, et al. A roadmap of constitutive NF-κB activity in Hodgkin lymphoma: Dominant roles of p50 and p52 revealed by genome-wide analyses. *Genome Medicine*. 2016;8(1). doi:10.1186/S13073-016-0280-5

44. Castinetti F, Reynaud R, Saveanu A, et al. MECHANISMS IN ENDOCRINOLOGY: An update in the genetic aetiologies of combined pituitary hormone deficiency. *European Journal of Endocrinology*. 2016;174(6):R239-R247. doi:10.1530/EJE-15-1095

45. Randolph LN, Jiang Y, Lian X, Randolph LN, Jiang Y, Lian X. Stem Cell Engineering and Differentiation for Disease Modeling and Cell-based Therapies. *CTE*. 2017;1(2):140-157. doi:10.3934/celltissue.2017.2.140

46. Schwank G, Koo BK, Sasselli V, et al. Functional repair of CFTR by CRISPR/Cas9 in intestinal stem cell organoids of cystic fibrosis patients. *Cell Stem Cell*. 2013;13(6):653-658. doi:10.1016/j.stem.2013.11.002

47. Takasato M, Er PX, Chiu HS, et al. Kidney organoids from human iPS cells contain multiple lineages and model human nephrogenesis. *Nature*. 2015;526(7574):564-568. doi:10.1038/nature15695

48. Guan Y, Xu D, Garfin PM, et al. Human hepatic organoids for the analysis of human genetic diseases. *JCI Insight*. 2017;2(17):e94954, 94954. doi:10.1172/jci.insight.94954

49. Moreira L, Bakir B, Chatterji P, Dantes Z, Reichert M, Rustgi AK. Pancreas 3D Organoids: Current and Future Aspects as a Research Platform for Personalized Medicine in Pancreatic Cancer. *Cellular and Molecular Gastroenterology and Hepatology*. 2018;5(3):289-298. doi:10.1016/j.jcmgh.2017.12.004

50. Nanki Y, Chiyoda T, Hirasawa A, et al. Patient-derived ovarian cancer organoids capture the genomic profiles of primary tumours applicable for drug sensitivity and resistance testing. *Sci Rep*. 2020;10(1):12581. doi:10.1038/s41598-020-69488-9

51. Kong J, Wen S, Cao W, et al. Lung organoids, useful tools for investigating epithelial repair after lung injury. *Stem Cell Research & Therapy*. 2021;12(1):95. doi:10.1186/s13287-021-02172-5

52. McEachern R, Drouin J, Metherell L, Huot C, Van Vliet G, Deal C. Severe Cortisol Deficiency Associated with Reversible Growth Hormone Deficiency in Two Infants: What Is the Link? *The Journal of Clinical Endocrinology & Metabolism*. 2011;96(9):2670-2674. doi:10.1210/jc.2011-0129

53. Liu Y, Hanson S, Gurugama P, Jones A, Clark B, Ibrahim MAA. Novel NFKB2 Mutation in Early-Onset CVID. *J Clin Immunol*. 2014;34(6):686-690. doi:10.1007/s10875-014-0064-x

54. Maccari ME, Scarselli A, Di Cesare S, et al. Severe Toxoplasma gondii infection in a member of a NFKB2-deficient family with T and B cell dysfunction. *Clinical Immunology*. 2017;183:273-277. doi:10.1016/j.clim.2017.09.011

55. Mac TT, Castinetti F, Bar C, et al. Anterior pituitary hormone deficiency in DAVID syndrome. *Journal of Neuroendocrinology*. 2023.

56. Tucker E, O'Donnell K, Fuchsberger M, et al. A novel mutation in the Nfkb2 gene generates an NF-kappa B2 "super repressor." *J Immunol*. 2007;179(11):7514-7522. doi:10.4049/jimmunol.179.11.7514

57. Cohen RN, Cohen LE, Botero D, et al. Enhanced Repression by HESX1 as a Cause of Hypopituitarism and Septooptic Dysplasia. *The Journal of Clinical Endocrinology & Metabolism*. 2003;88(10):4832-4839. doi:10.1210/jc.2002-021868

58. Ohuchi H, Hori Y, Yamasaki M, et al. FGF10 acts as a major ligand for FGF receptor 2 IIIb in mouse multi-organ development. *Biochem Biophys Res Commun*. 2000;277(3):643-649. doi:10.1006/bbrc.2000.3721

59. Ericson J, Norlin S, Jessell TM, Edlund T. Integrated FGF and BMP signaling controls the progression of progenitor cell differentiation and the emergence of pattern in the embryonic anterior pituitary. *Development*. 1998;125(6):1005-1015. doi:10.1242/dev.125.6.1005

60. Giraldi FP, Cassarino F, Pagliardini L, Asnaghi V, Cavagnini F. The human POMC gene promoter: Where do we stand? *J Endocrinol Invest*. 2011;34(6):454-460. doi:10.1007/BF03346713

61. Drouin J. 60 YEARS OF POMC: Transcriptional and epigenetic regulation of POMC gene expression. *Journal of Molecular Endocrinology*. 2016;56(4):T99-T112. doi:10.1530/JME-15-0289

62. De Donatis GM, Le Pape E, Pierron A, et al. NF-kB2 induces senescence bypass in melanoma via a direct transcriptional activation of EZH2. *Oncogene*. 2016;35(21):2735-2745. doi:10.1038/onc.2015.331

63. Stallings CE, Das P, Athul SW, Ukagwu AE, Jensik PJ, Ellsworth BS. FOXO1 regulates expression of Neurod4 in the pituitary gland. *Molecular and Cellular Endocrinology*. 2024;583:112128. doi:10.1016/j.mce.2023.112128

64. Sasaki H, Suga H, Takeuchi K, et al. Subcutaneous transplantation of human embryonic stem cells-derived pituitary organoids. *Frontiers in Endocrinology*. 2023;14. Accessed April 12, 2023. https://www.frontiersin.org/articles/10.3389/fendo.2023.1130465

65. Taga S, Suga H, Nakano T, et al. Generation and purification of ACTH-secreting hPSC-derived pituitary cells for effective transplantation. *Stem Cell Reports*. 2023;18(8):1657-1671. doi:10.1016/j.stemcr.2023.05.002

Figure legends

Figure 1: Design of sgRNA and ssODN to edit in the *TBX19*^{K146R} mutation

A, Illustration of the *TBX19* gene (HGNC: 11596; ENSEMBL: ENSG00000143178; Human GRCh38) and TBX19 protein.

B, Wild-type (WT) sequence containing target site, cut site, target and PAM sequences.

C, ssODN design to edit in a missense K146R mutant of *TBX19* using CRISPR/Cas9.

D, Sequence analysis of a *TBX19* KI hiPSC clone 63 obtained by Sanger sequencing after screening by CAPS. This clone was subsequently used in this work to differentiate into pituitary organoids (see below).

E, Summary of our strategy procedure:

Step 1: Production of the knock-in hiPSC lines by CRISPR/Cas9 genome editing.

Step 2: Differentiation into pituitary organoids from mutant hiPSC lines in parallel with the isogenic WT line using 3D culture, followed by comparison of the development of organoids between the two groups.

Figure 2: **Time course of organoid growth and gene expression in WT and *TBX19* KI organoids**

A, Culture protocol and outline to generate pituitary organoids in three-dimensional (3D) culture from hiPSC. Organoids were collected at days (d) 0, 6, 18, 27, 48, 75, 105 during differentiation to analyze.

B, Bright-field microscopy views of WT organoid examples at different time points throughout differentiation. Scale bars indicated in each image.

C, Number of replicates per time point and per genotype in experiments depicted in following graphs. Asterisks indicate that 7-8 organoids were grouped for each sample. For other points, each sample consists of a single organoid.

D-H, Relative quantification (RQ) mRNA expression analysis for key markers of pituitary organoids during differentiation: WT (in black line) and *TBX19* KI organoids (in red line). Relative quantification of each target gene was obtained by the $2^{-\Delta\Delta Ct}$ method from qRT-PCR results (see Methods). Data show means ± standard error of the mean (SEM, Mann-Whitney t-test [unpaired, two-tailed, nonparametric]). $p < 0.05$ (*), $p < 0.01$ (**).

D, Relative quantification of *HESX1* expression, the earliest pituitary placode marker assessed. The expression of *HESX1* is significantly downregulated in *TBX19* KI organoids vs. WT at d18 and d27.

E, Relative quantification expression of *PITX1*, a pituitary progenitor marker. *PITX1* was significantly downregulated in *TBX19* KI organoids by d48 and d75.

F, Relative quantification expression of *LHX3*, a pituitary progenitor marker. *LHX3* was significantly lower in *TBX19* KI organoids as compared to WT from d48 onwards.

G, Relative quantification expression of *TBX19*, a critical transcriptional determinant for corticotroph differentiation. *TBX19* expression is higher in *TBX19* KI organoids at d105.

H, Relative quantification expression of *POMC*, a corticotroph marker. *POMC* was significantly downregulated in *TBX19* KI organoids from d48 onwards.

Figure 3: Impairment of corticotroph development in *TBX19* KI organoids as compared with controls at the protein level

A, B, Immunostaining of LHX3 and CDH1 (E-cadherin) expression in epithelial cells, typical of Rathke's pouch ectoderm in early pituitary primordia, was reduced in *TBX19* KI organoid *vs* WT on day 48 (n=10 organoids for each group). Scale bars: 10 μm.

C, D, Immunostaining showed that ACTH and TBX19 expressions were reduced in *TBX19* KI organoid *vs* WT on day 105 (n=10 organoids for each group). Scale bars: 10 μm.

Figure 4: **3D reconstruction of whole wild-type (WT) and *TBX19* KI organoids on day 105**

A, A representative image of whole-mount immunostaining against ACTH in a cleared WT organoid on d105 using light-sheet microscopy. Scale bar: 200 µm.

B, A representative image of whole-mount immunostaining against ACTH in a cleared *TBX19* KI organoid on d105 as above, showing impaired corticotroph differentiation. Scale bar: 200 µm.

C, The number of corticotroph cells per mm^3 was significantly decreased in *TBX19* KI organoids (* p= 0.0159). Means ± *SEM* for n=4 WT, n=5 *TBX19* KI organoids. Mann-Whitney test (unpaired, two-tailed, nonparametric).

Figure 5: Design of sgRNA and ssODN to introduce a *NFKB2*^{D865G} mutation

A, Illustration of the *NFKB2* gene (HGNC: 7795; ENSEMBL: ENSG00000077150; Human GRCh38).

B, WT sequence containing target site, cut site, target and PAM sequence.

C, ssODN design to introduce the missense mutation D865G into *NFKB2* using CRISPR/Cas9.

D, Sequence analysis of the *NFKB2* KI hiPSC clone 7, obtained by Sanger sequencing, after screening by CAPS. This clone was subsequently used in this work to differentiate into pituitary organoids (see below).

Figure 6: **Time course of organoid growth and gene expression in WT and *NFKB2* KI organoids**

A, Number of replicates per time point and per genotype in experiments depicted in following graphs. Asterisks indicate that 7-8 organoids were grouped for each sample. For other point, each sample consists of a single organoid.

B-F, Relative quantification (RQ) mRNA expression analysis for key markers of pituitary organoids during differentiation: WT (black line and dots) and *NFKB2* KI organoids (red line and dots). Data show means ± standard error of the mean (SEM);. Mann-Whitney t-test (unpaired, two-tailed, nonparametric). $p < 0.05$ (*), $p < 0.01$ (**).

B, Relative quantification expression of *HESX1*, the earliest pituitary placode marker assessed. The expression of *HESX1* was upregulated in *NFKB2* KI organoids vs. WT between d27 and d75.

C, Pituitary progenitor marker *PITX1* was significantly downregulated in *NFKB2* KI organoids at d48 and d75.

D, Pituitary progenitor marker *LHX3* was significantly lower in *NFKB2* KI organoids as compared to WT from d48 onwards.

E, Relative quantification expression of *TBX19*, a corticotroph marker. *TBX19* was significantly increased in *NFKB2* KI organoids by d105.

F, Relative quantification expression of *POMC*, a corticotroph marker. *POMC* was significantly downregulated in *NFKB2* KI organoids from d75.

G, Volume of organoids (mm^3) on d105, calculated using Imaris software (see in methods). There was no significant difference in volume between WT and *NFKB2* KI organoids ($p = 0.6126$). Data show means ± *SEM*; n=7 in the WT group, n=8 in the mutant group. Mann-Whitney test (unpaired, two-tailed).

Figure 7: Impairment of pituitary development in *NFKB2* KI organoids

A, B, Immunostaining for LHX3 (green) and p100/p52 (red) in the early pituitary-type epithelium was reduced in *NFKB2* KI organoids vs WT on day 48 (n=10 organoids for each group). Stronger expression of p100/p52 was observed in pituitary progenitors, but expression in the hypothalamic part of the organoid cannot be excluded. Scale bar: 10 µm

C, D, by day 105, although nuclear TBX19 was detectable in both mutants, these cells failed to co-express ACTH in *NFKB2* KI organoids (n=10 organoids for each group). Scale bars: 10 µm

Figure 8: **3D reconstruction of whole Wild type (WT) and *NFKB2* KI organoids on day 105**

A, A representative image of whole-mount immunostaining against ACTH in a cleared WT organoid on d105 using light-sheet microscopy. Scale bar: 200 μm.

B, A representative image of whole-mount immunostaining against ACTH in a cleared *NFKB2* KI organoid on d105 as above, showing impaired corticotroph differentiation. Scale bar: 100 μm.

C, The number of corticotroph cells per mm^3 was significantly decreased in *NFKB2* KI organoids (* p= 0.0007). Means ± *SEM* for n=6 organoids WT, n=8 *NFKB2* KI organoids. Mann-Whitney test (unpaired, two-tailed, nonparametric).

Figure 9: **Whole-transcriptome profiles of WT vs *NFKB2* KI organoids on day 48**

A, Heat map showing global differential gene expression between WT vs *NFKB2* KI organoids (n=5 for each group).

B, Volcano plot of genes showing differential gene expression between WT vs *NFKB2* KI organoids (expressed in Log_2 fold-change). Blue dots in the left panel indicate 144 genes involved in hypothalamic-pituitary development. Grey dots indicate all other genes detected in RNA-seq.

C, Volcano plot of genes showing differential gene expression between WT vs *NFKB2* KI organoids. Green dots indicate genes coding for 39 key transcription factors whose expression is significantly changed (padj < 0.05). Red dots indicate key transcription factors with non-significant changes (padj> 0.05). Grey dots indicate all other genes detected in RNA-seq.

Figure 10: Impaired pituitary progenitor development is correlated with changes in growth factor expression in *NFKB2* KI organoids

A, RT-qPCR experiments at d48 showing that *HESX1* expression is upregulated *NFKB2* KI organoids, compared to WT and *TBX19* KI, whereas *PITX1* and *LHX3* are downregulated in both mutants.

B, *BMP4* expression is increased whereas and *FGF8* and *FGF10* are decreased in *NFKB2* mutants, but unchanged in *TBX19* KI organoids.

Data show means ± *SEM*; n=17, 12 and 11 for WT, *TBX19* KI and *NFKB2* KI respectively. Mann-Whitney t-test (unpaired, two-tailed, nonparametric). $p < 0.05$ (*), $p < 0.01$ (**), $p<0.005$ (***),

Figure 11: Impaired differentiation of corticotrophs in *TBX19* KI and *NFKB2* KI organoids

A, RT-qPCR measurements of *TBX19* expression show a late (d105) increase in both mutants, with stronger effect in *TBX19* KI organoids.

B, Corticotroph terminal differentiation marker *NR4A2* was decreased in both mutants at d48 and d75, but only in *NFKB2* mutants at d105.

C, *PCSK1* downregulation is only observed in *NFKB2* KI at d48, and in both models at d75 and d102.

D, A decrease in *POMC* expression is observed in both mutants from d48 onwards.

Data show means ± *SEM*; d48: n=17, 12 and 11; d75, n=9, 7 and 6 ; d105: n=9, 5 and 5 for WT, *TBX19* KI and *NFKB2* KI organoids respectively. Mann-Whitney t-test (unpaired, two-tailed, nonparametric). $p < 0.05$ (*), $p < 0.01$ (**), $p<0.005$ (***),

Figure 12: POU1F1-dependent lineages are affected in *TBX19* KI and *NFKB2* KI organoids

A, Strong downregulation of *PROP1* expression is observed at d48 in both mutants and persists at d75.

B, Expression of POU1F1-dependant lineage progenitors and mature somatotrophs marker *NEUROD4* is decreased at d48 inNFKB2 organoids, and in both models at d105.

C, *ZBTB20*, a marker for POU1F1-dependant lineage progenitors and mature lactotrophs, is less expressed in *NFKB2* KI organoids at d48, but at normal levels by d75. In *TBX19* KI mutants, its expression is normal at d48 but decreased by d75.

D, On d75, *POU1F1* expression is barely detectable in either model.

Data show means ± *SEM*; d48: n=17, 12 and 11; d75: n=9, 7 and 6 for WT, *TBX19* KI and *NFKB2* KI organoids respectively. Mann-Whitney t-test (unpaired, two-tailed, nonparametric). $p < 0.05$ (*), $p < 0.01$ (**), $p<0.005$ (***).

Figure 13: Identification of genes potentially under direct p52 regulation

Venn diagram showing the total number and intersections of genes identified as p52 targets, genes differentially expressed at d48 between WT and *NFKB2* KI organoids, and a literature-curated list of genes particularly implicated in hypothalamus-pituitary development. The table on the right shows the identity of the 23 genes (circled in red), with color code indicating whether they are upregulated (green) or downregulated (pink) in *NFKB2* KI mutants at d48.

Figure 14: Changes in gene expression induced by *NFKB2*$^{D865G/D865G}$ mutation during hypothalamic-pituitary organoid development

Diagram illustrating changes in gene expression (black arrows) associated with different stages of normal hypothalamic-pituitary organoids development and cell differentiation. The *NFKB2*$^{D865G/D865G}$ mutation perturbs these changes (red arrow), possibly through direct transcriptional control for genes indicated in blue.

Table Legends

Table 1: RNA-seq expression data for a list of 144 genes known from the literature to have a functional influence on pituitary-hypothalamic development. Differentially expressed genes (padj < 0.05) in *NFKB2* KI organoids are highlighted in green when upregulated and in pink when downregulated.

Table 2: Differential gene expression analysis for genes associated with different stages of epithelial-to-mesenchymal transition in *NFKB2* KI vs WT organoids. Significantly decreased and increased expressions are highlighted in pink and green, respectively.

A *TBX19* gene

TBX19^{K146R} (AaG > AgG)

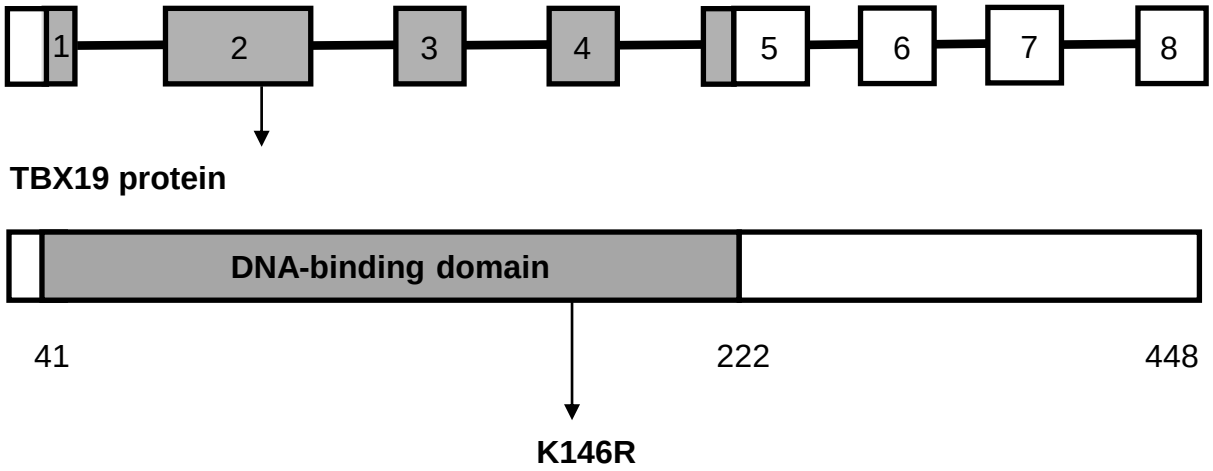

B WT

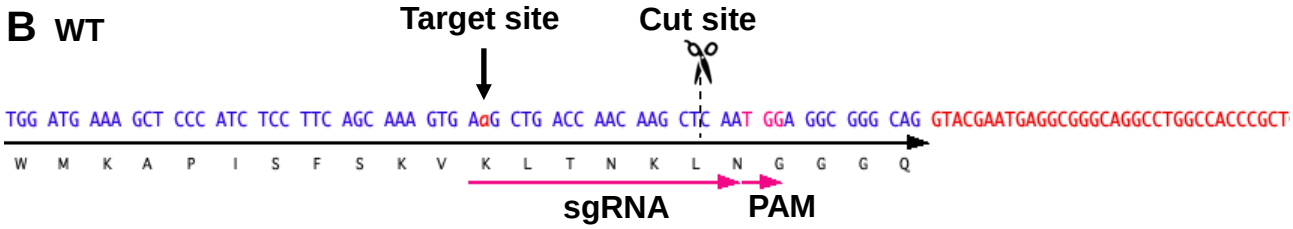

C ssODN

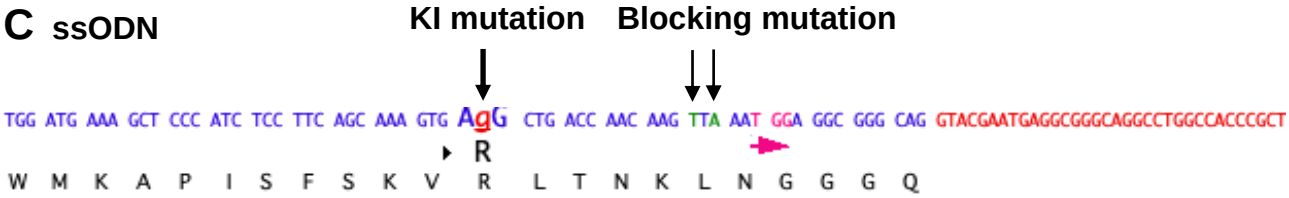

D

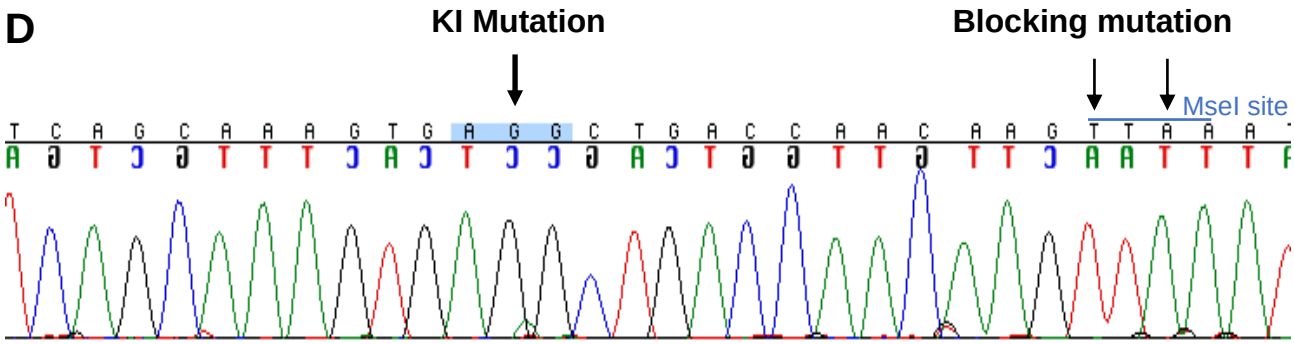

E

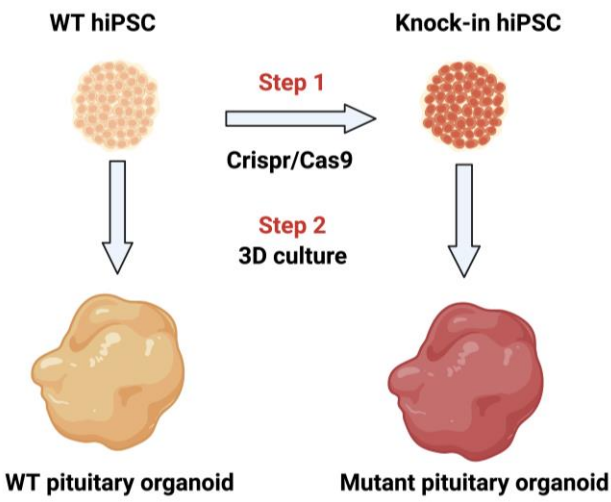

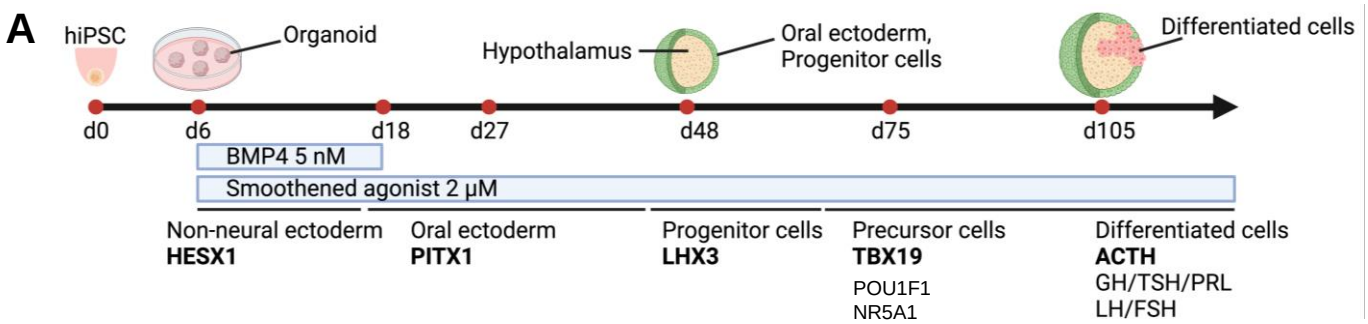

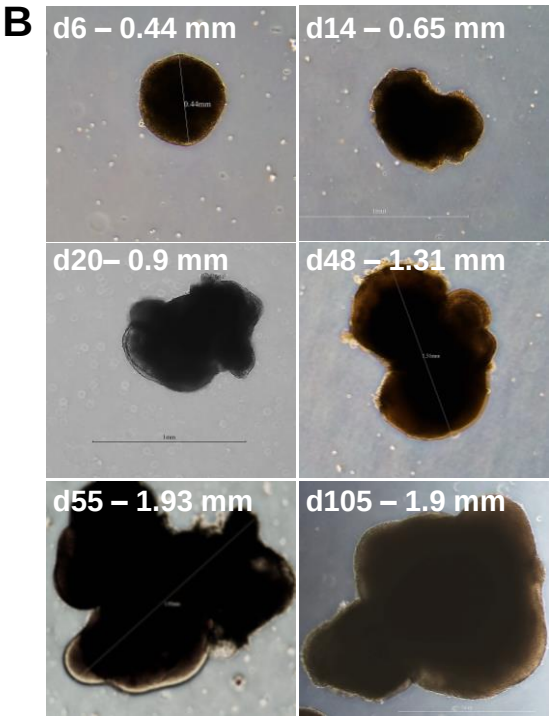

C

Number of replicates per experiment

	d0	d6	d18	d27	d48	d75	d105
WT	2*	6*	6*	9	12	10	10
TBX19-KI	2*	6*	6*	13	11	11	10

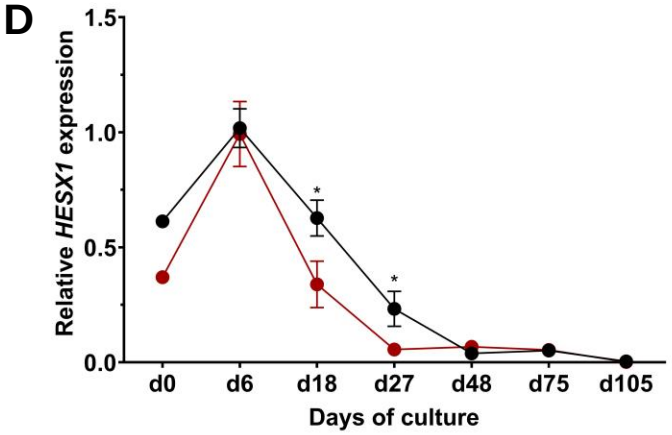

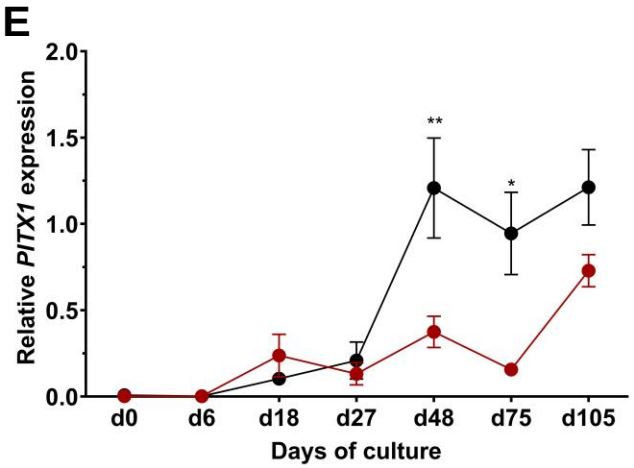

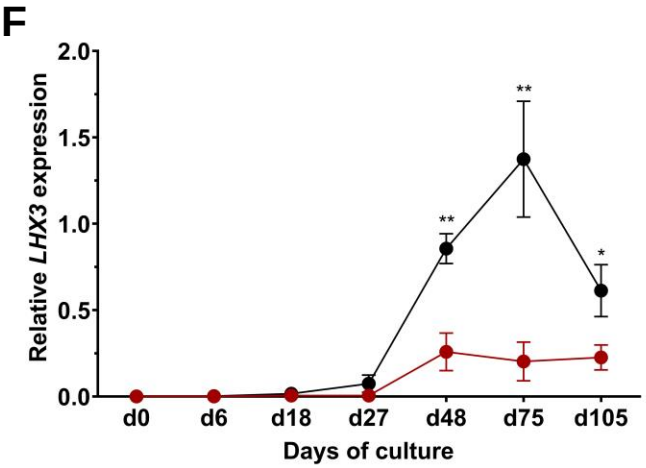

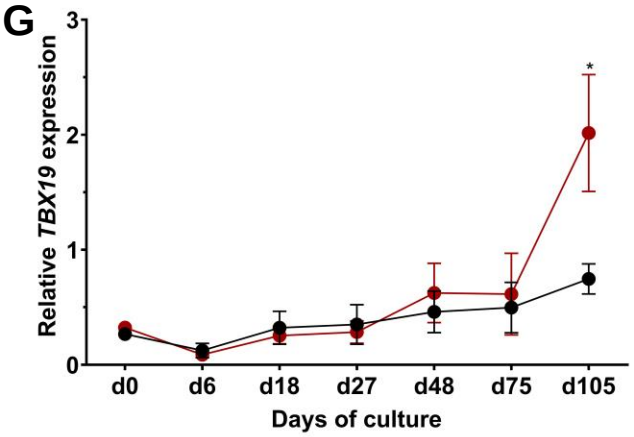

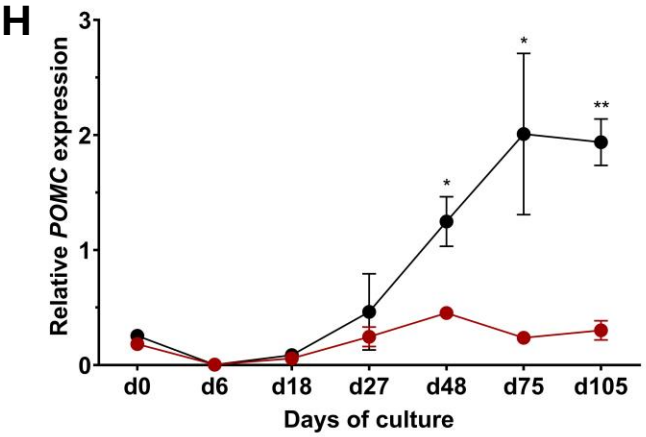

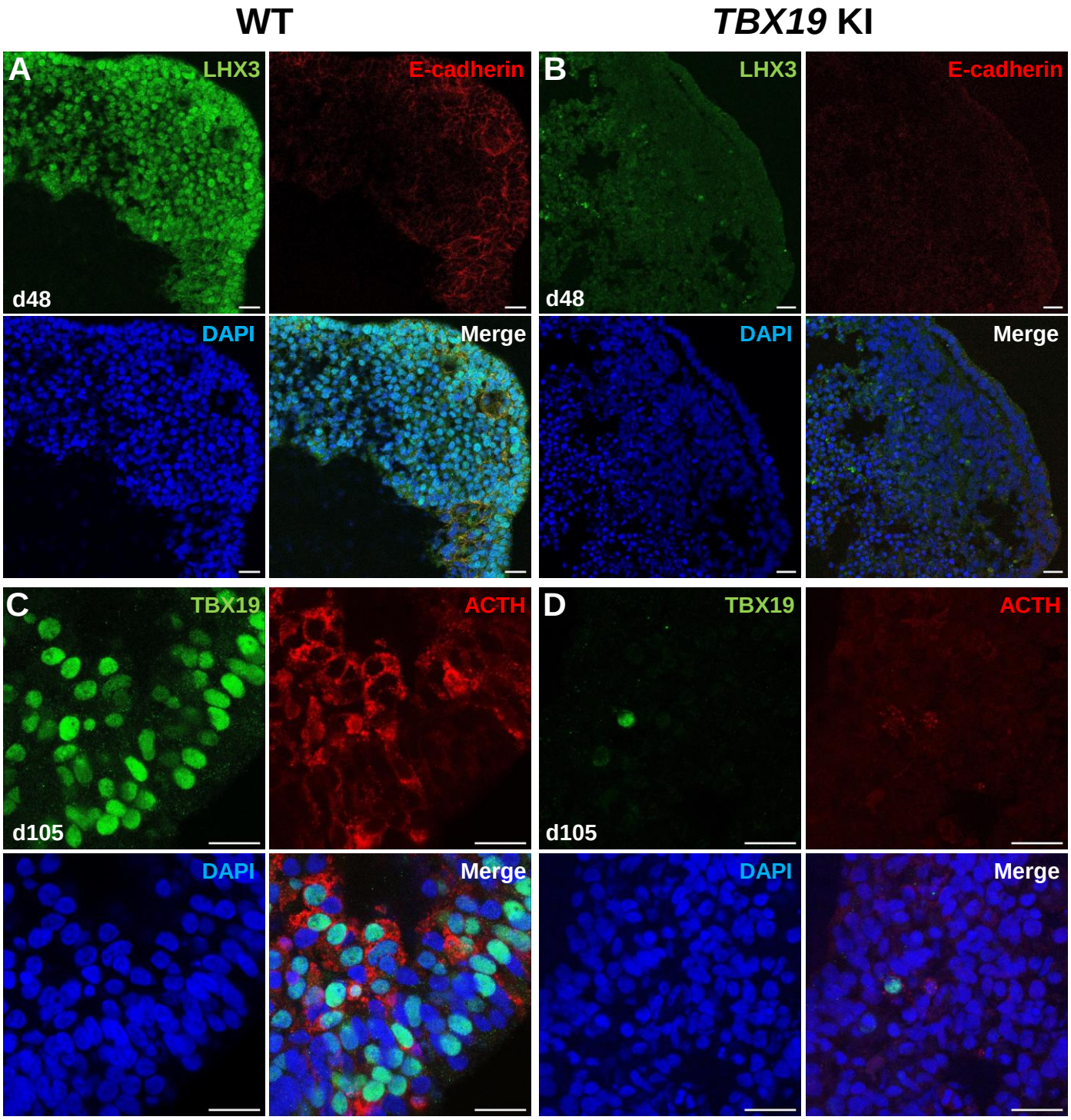
WT
TBX19 KI
A
LHX3
E-cadherin
d48
DAPI
Merge
B
LHX3
E-cadherin
d48
DAPI
Merge
C
TBX19
ACTH
d105
DAPI
Merge
D
TBX19
ACTH
d105
DAPI
Merge

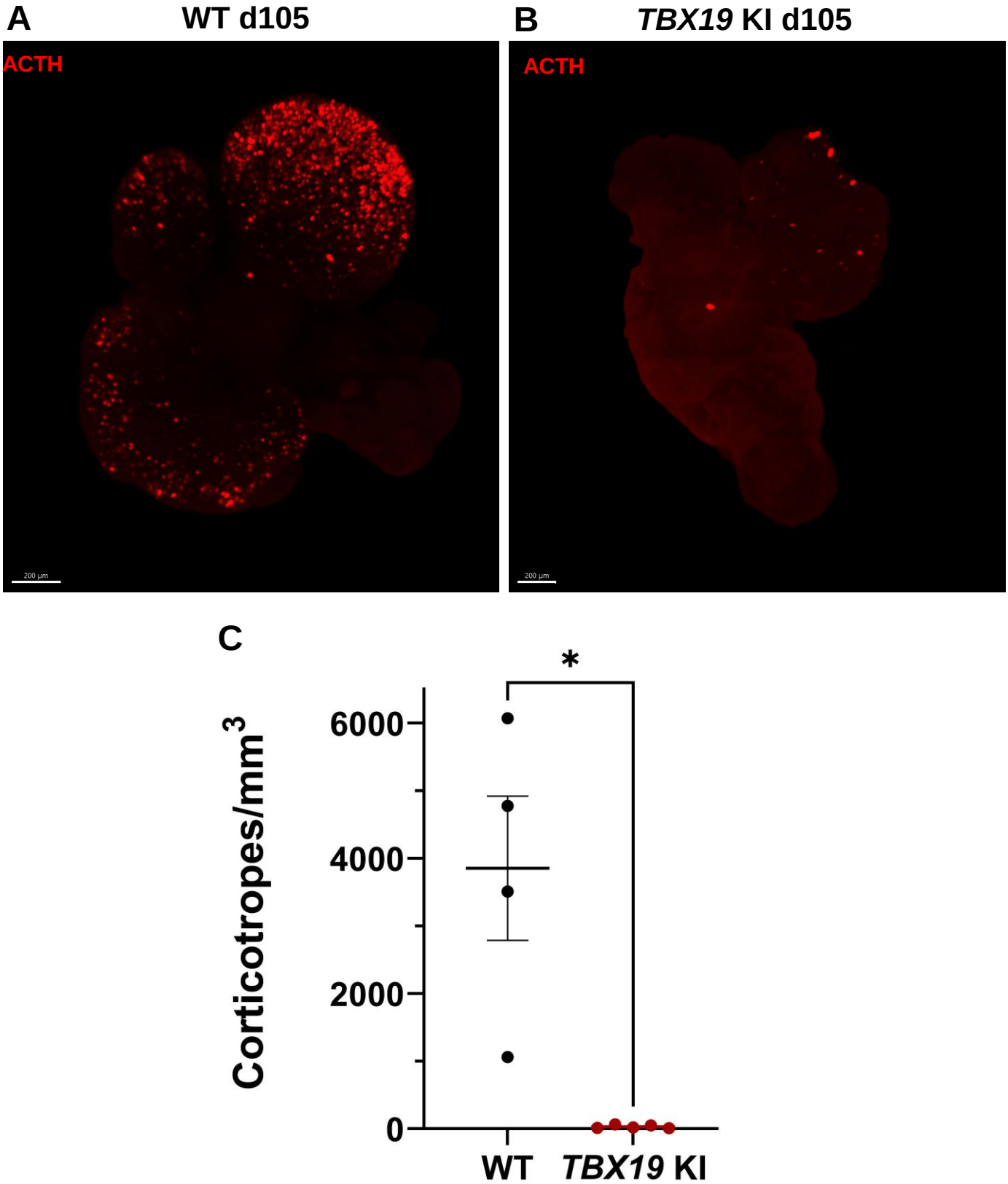
A
WT d105
ACTH
200 µm
B
TBX19 KI d105
ACTH
200 µm
C
*
Corticotropes/mm3
6000
4000
2000
0
WT
TBX19 KI

A ***NFKB2* gene**

NFKB2^{D865G} **(GaC > GgC)**

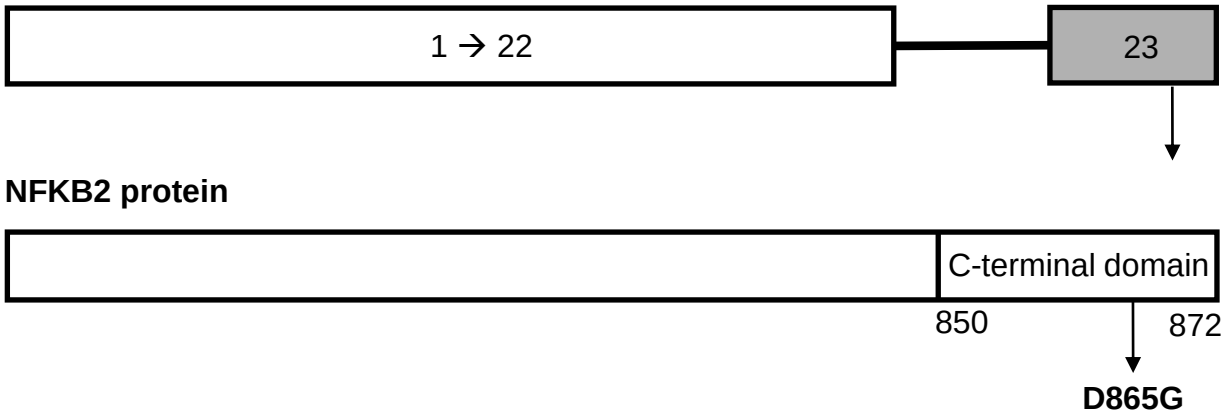

B **WT**

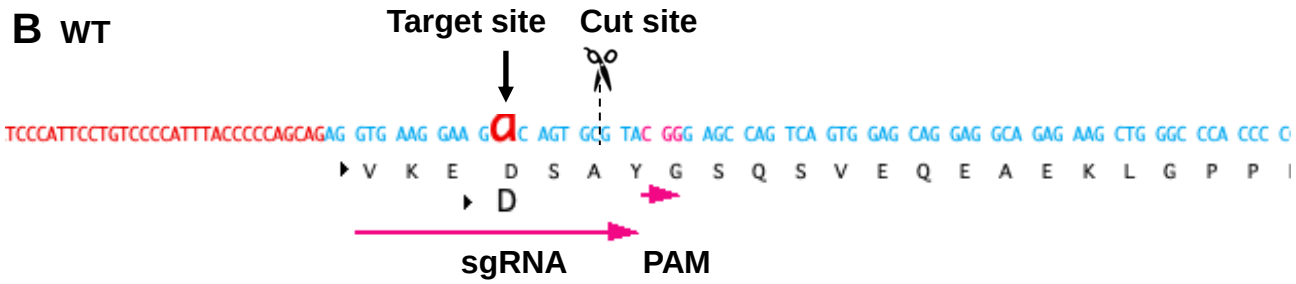

C **ssODN**

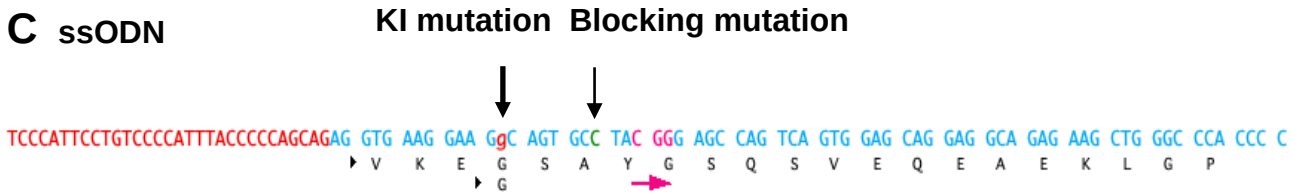

D

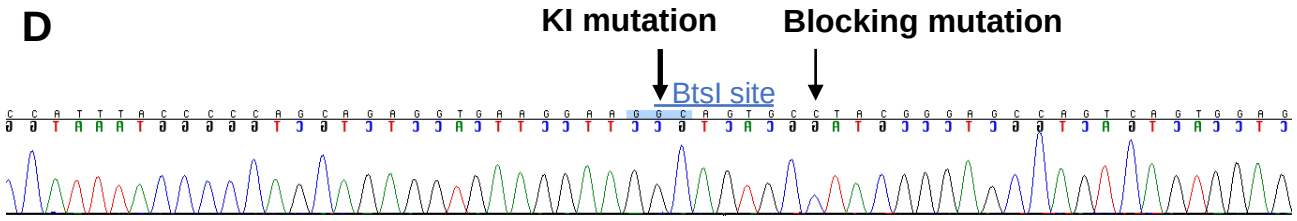

A

Number of replicates per experiment

	d0	d6	d18	d27	d48	d75	d105
WT	2*	6*	6*	9	10	9	10
***NFKB2*- KI**	2*	6*	6*	9	11	11	11

B

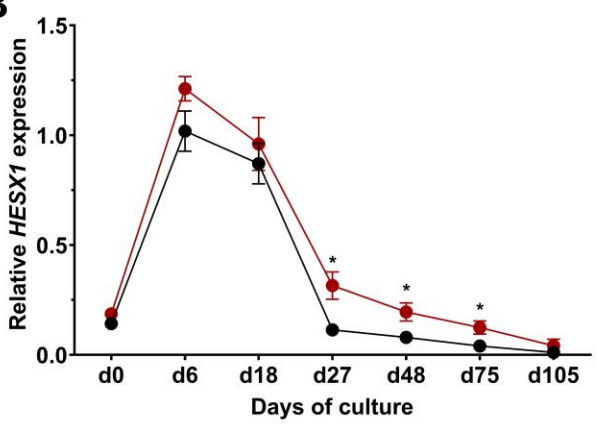

C

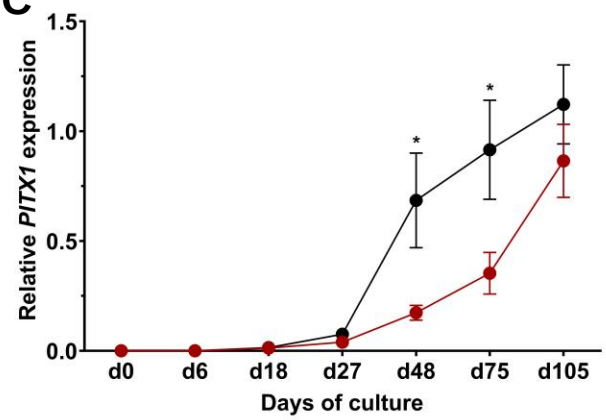

D

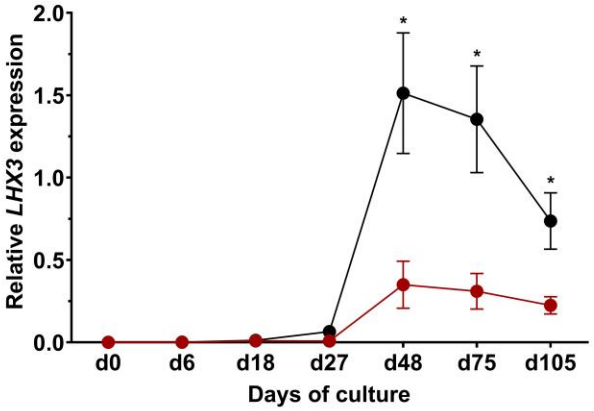

E

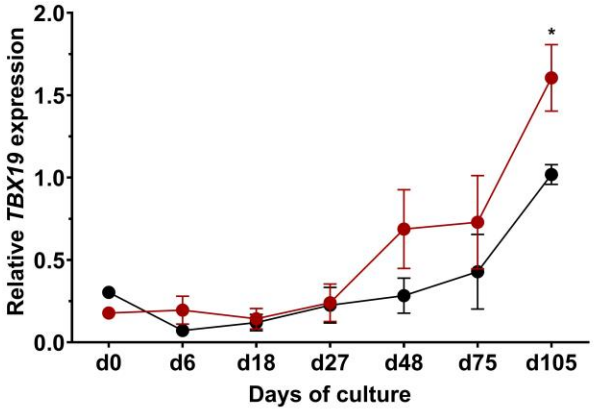

F

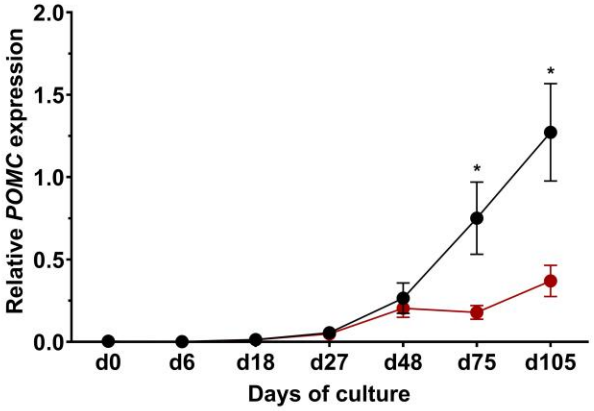

G

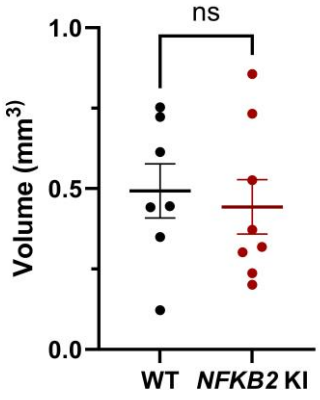

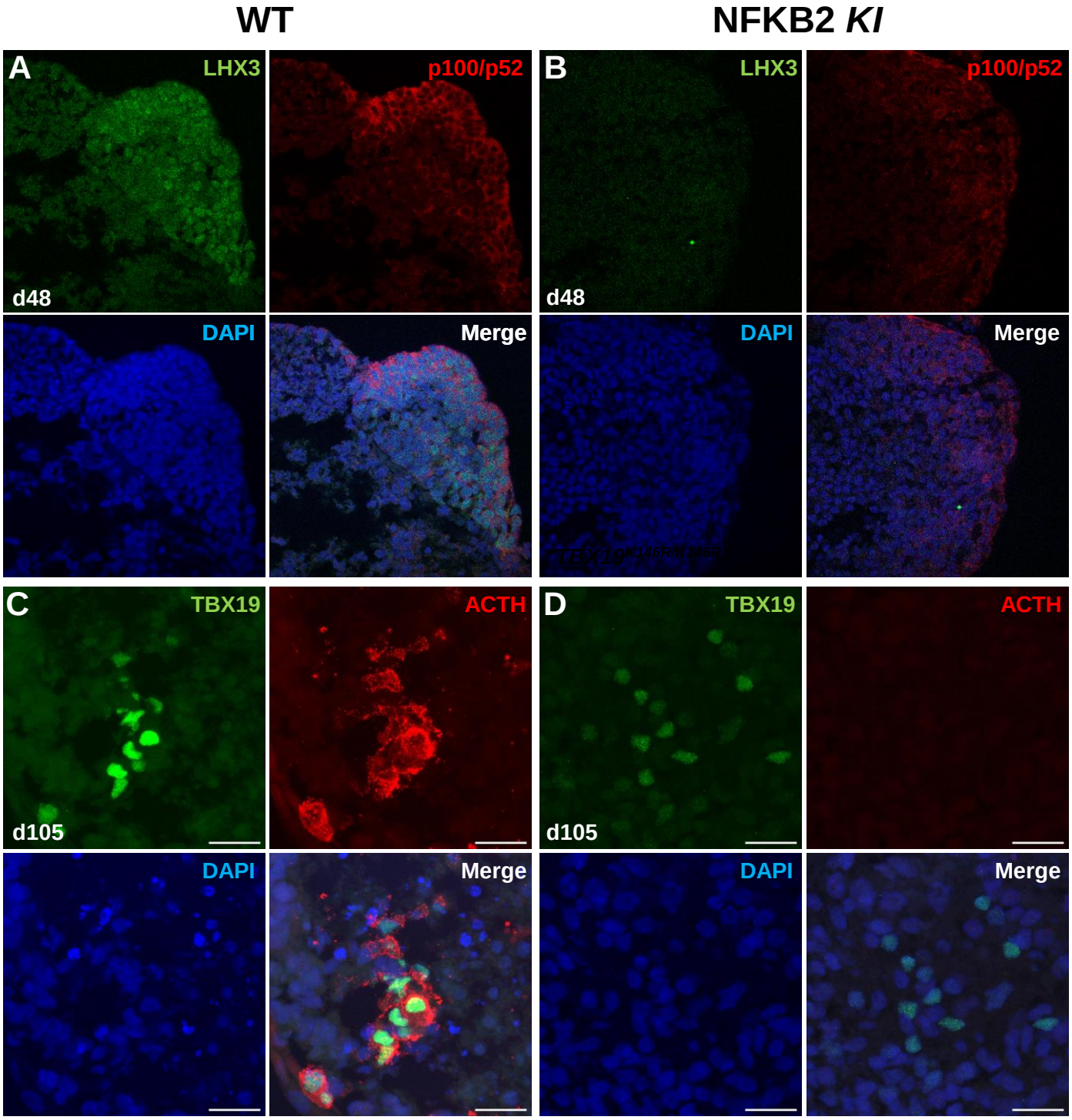
WT
NFKB2 KI
A
LHX3
p100/p52
d48
DAPI
Merge
B
LHX3
p100/p52
d48
DAPI
Merge
TBX19K146R/K146R
C
TBX19
ACTH
d105
DAPI
Merge
D
TBX19
ACTH
d105
DAPI
Merge

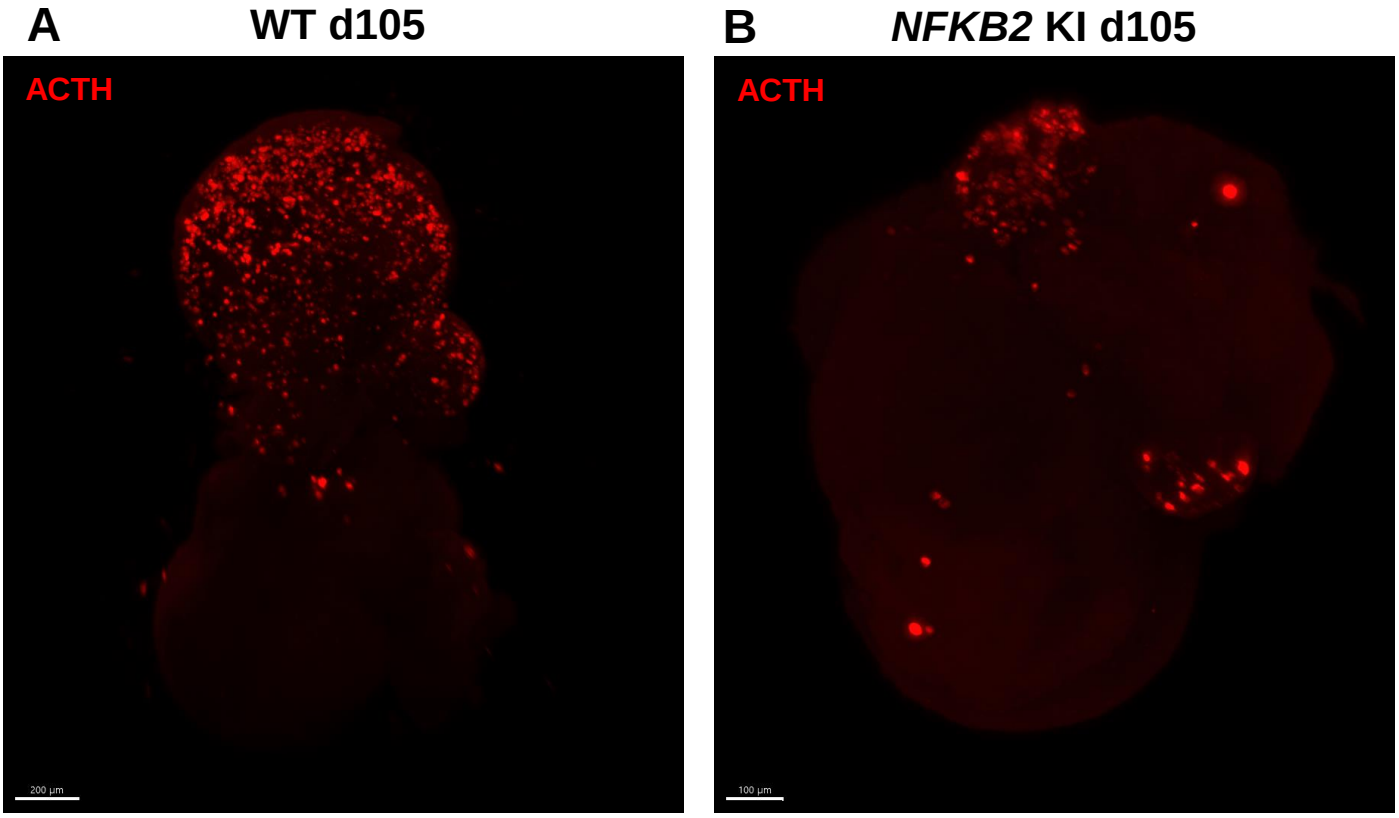
A
WT d105
ACTH
200 µm
B
NFKB2 KI d105
ACTH
100 µm

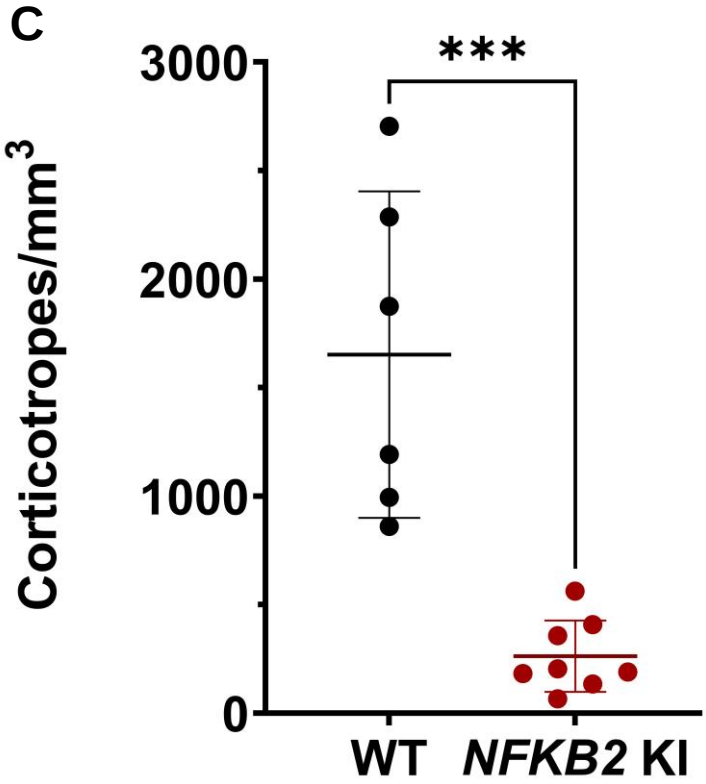
C
***
3000
2000
1000
0
Corticotropes/mm3
WT
NFKB2 KI

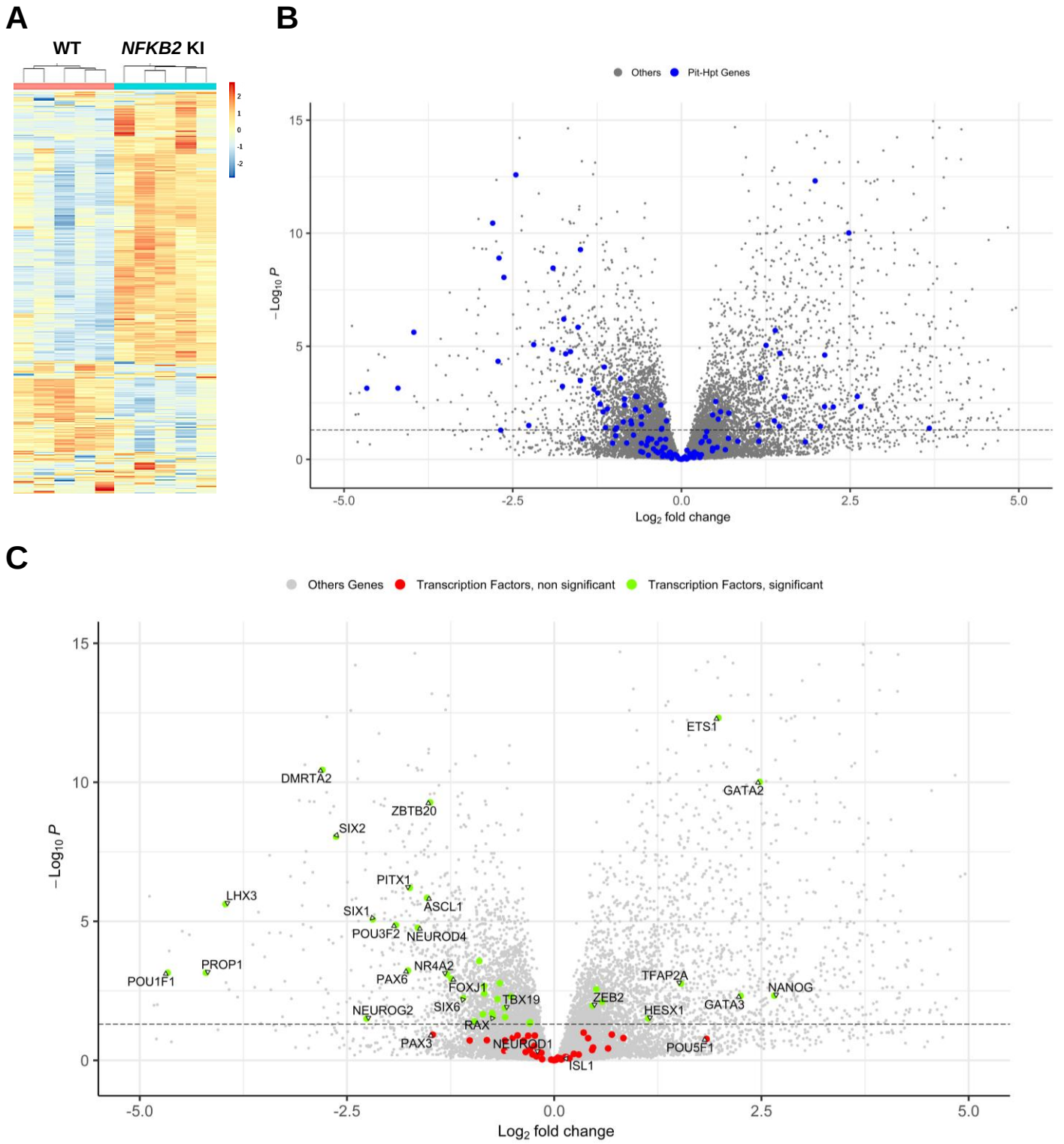
A
WT
NFKB2 KI
2
1
0
-1
-2
B
Others
Pit-Hpt Genes
15
10
5
0
−Log10 P
-5.0
-2.5
0.0
2.5
5.0
Log2 fold change
C
Others Genes
Transcription Factors, non significant
Transcription Factors, significant
ETS1
DMRTA2
GATA2
ZBTB20
SIX2
PITX1
LHX3
ASCL1
SIX1
POU3F2
NEUROD4
PROP1
NR4A2
POU1F1
PAX6
FOXJ1
TFAP2A
NANOG
TBX19
ZEB2
SIX6
NEUROG2
HESX1
GATA3
RAX
PAX3
NEUROD1
POU5F1
ISL1

d48

A

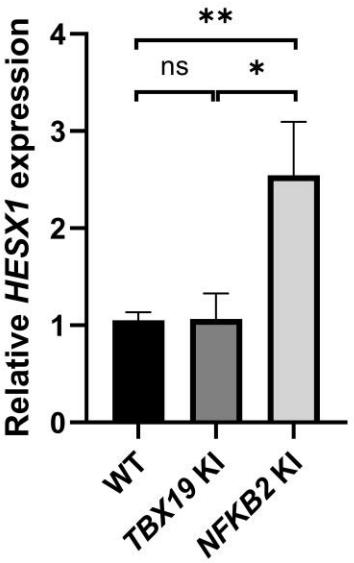
Relative HESX1 expression
0
1
2
3
4
**
ns
*
WT
TBX19 KI
NFKB2 KI

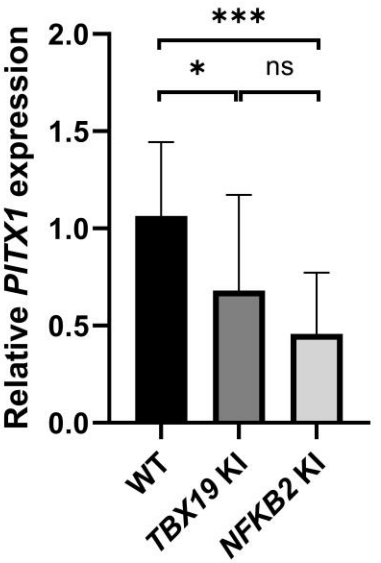
Relative PITX1 expression
0.0
0.5
1.0
1.5
2.0
***
*
ns
WT
TBX19 KI
NFKB2 KI

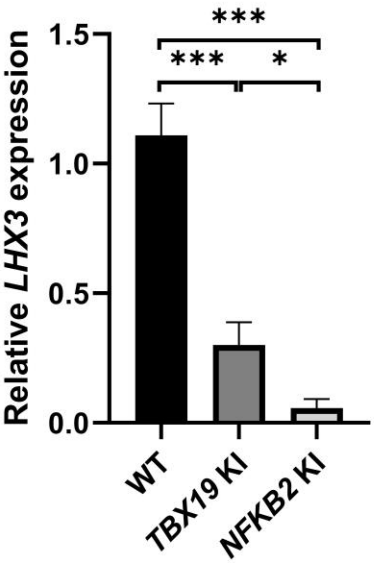
Relative LHX3 expression
0.0
0.5
1.0
1.5
***
***
*
WT
TBX19 KI
NFKB2 KI

B

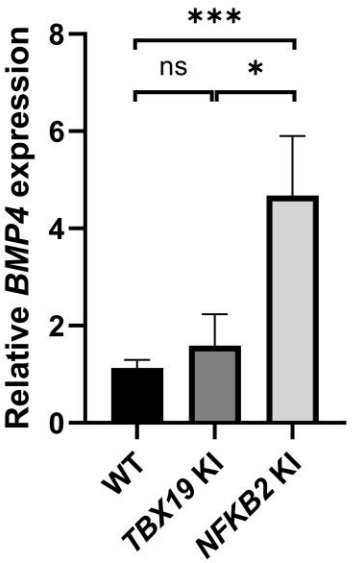
Relative BMP4 expression
0
2
4
6
8
***
ns
*
WT
TBX19 KI
NFKB2 KI

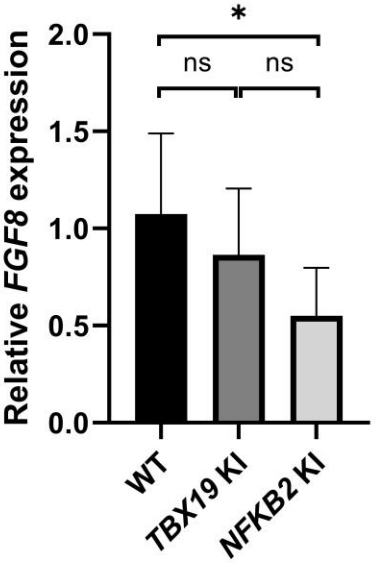
Relative FGF8 expression
0.0
0.5
1.0
1.5
2.0
*
ns
ns
WT
TBX19 KI
NFKB2 KI

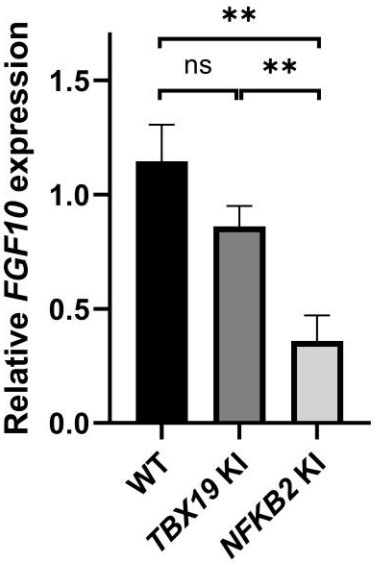
Relative FGF10 expression
0.0
0.5
1.0
1.5
**
ns
**
WT
TBX19 KI
NFKB2 KI

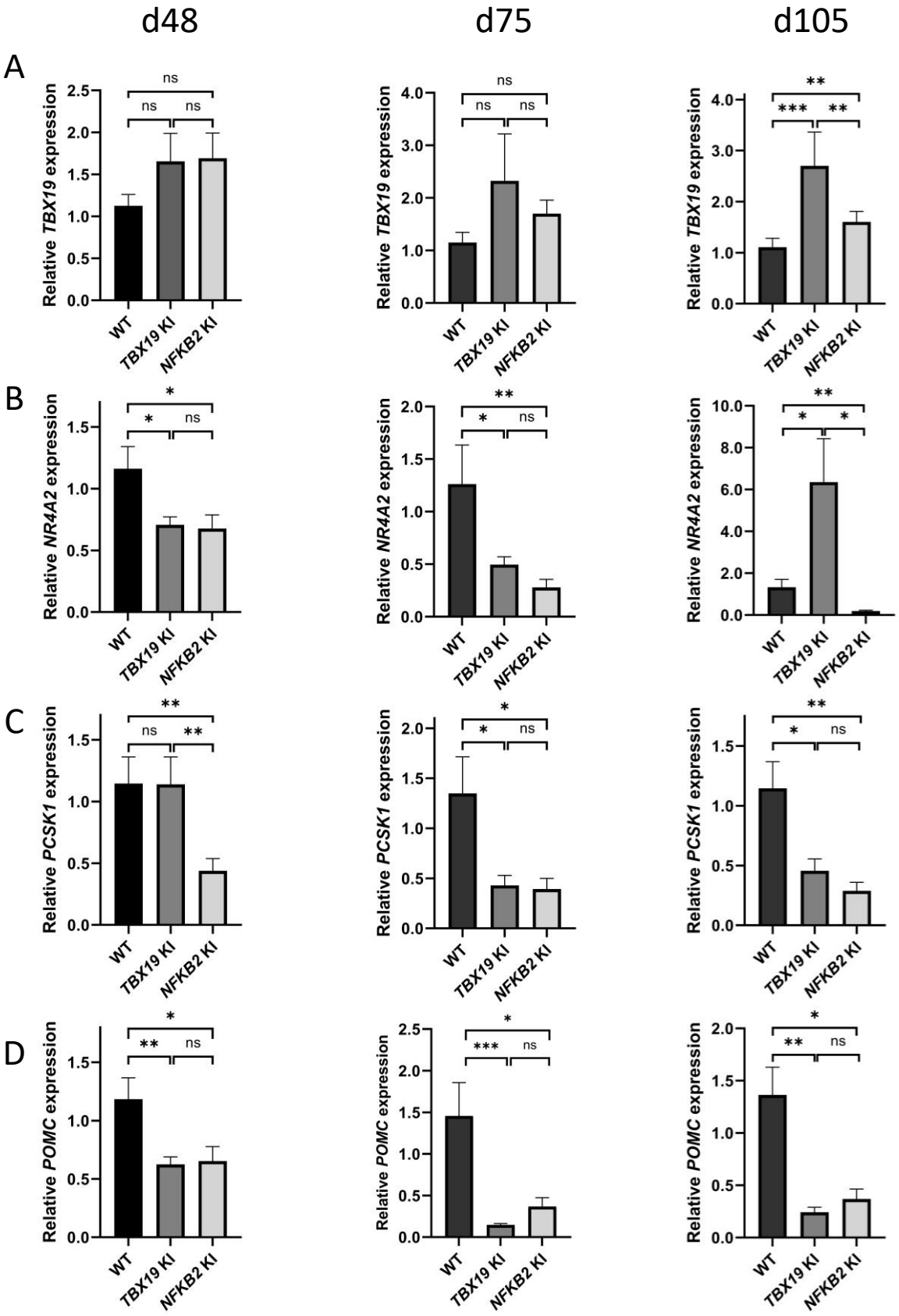
d48
d75
d105
A
B
C
D
Relative TBX19 expression
Relative NR4A2 expression
Relative PCSK1 expression
Relative POMC expression
WT
TBX19 KI
NFKB2 KI
ns
*
**
***

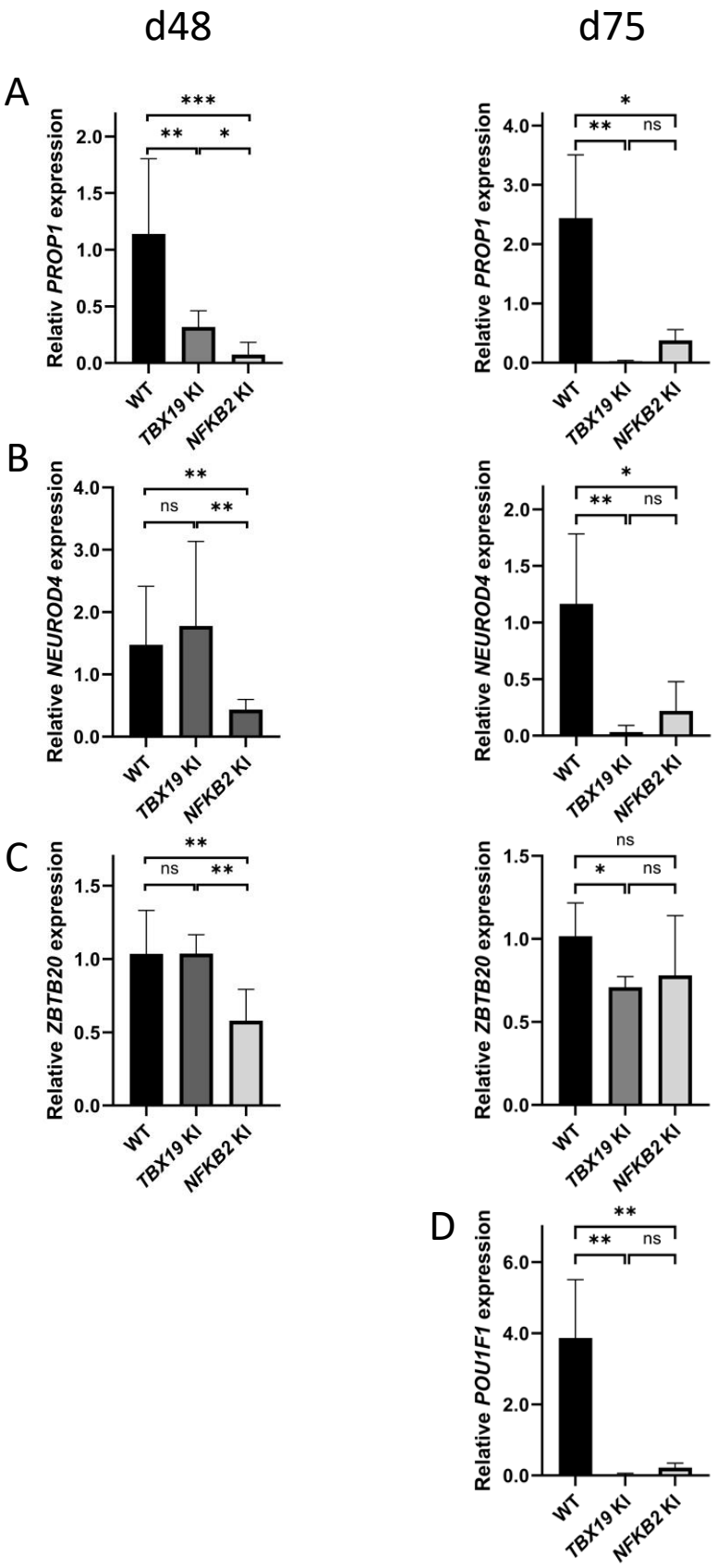
d48
d75
A
Relativ PROP1 expression
Relative PROP1 expression
B
Relative NEUROD4 expression
C
Relative ZBTB20 expression
D
Relative POU1F1 expression
WT
TBX19 KI
NFKB2 KI
***
**
*
ns

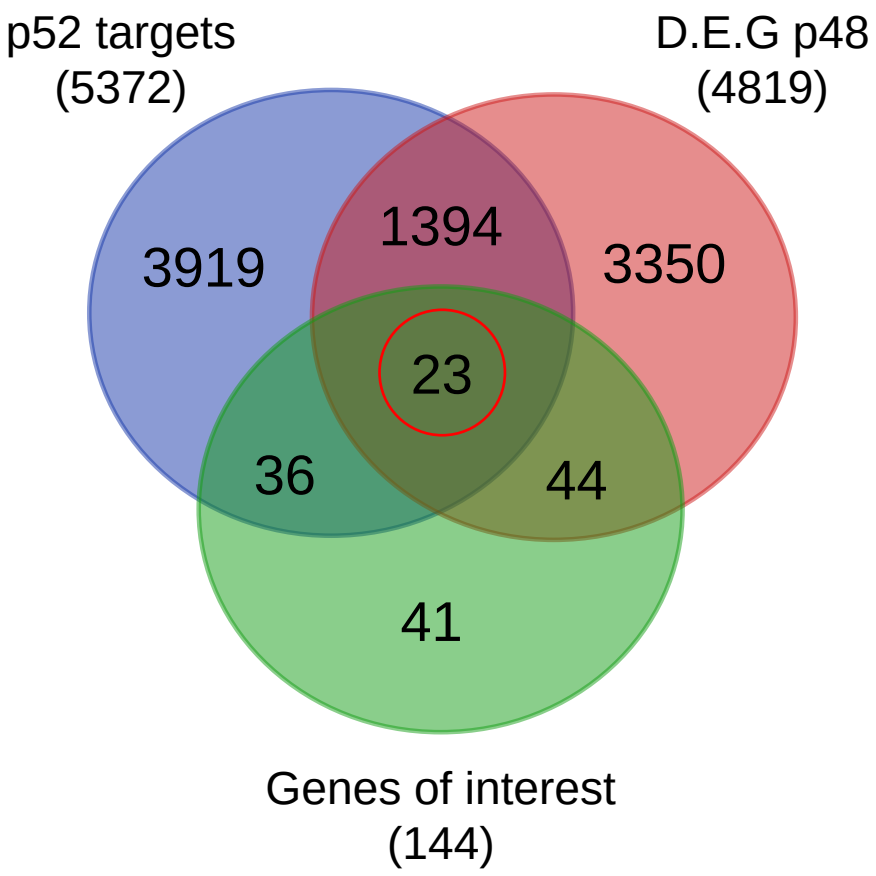

CDH1
CGA
CYP11A1
DRD2
ETS1
FOXO1
GATA3
LHX2
LHX4
NEUROD4
NEUROG2
NR4A2
PCSK1
PITX1
POMC
PROP1
RBPJ
SIX2
SOX9
TBX19
TGIF1
THRB
ZEB2

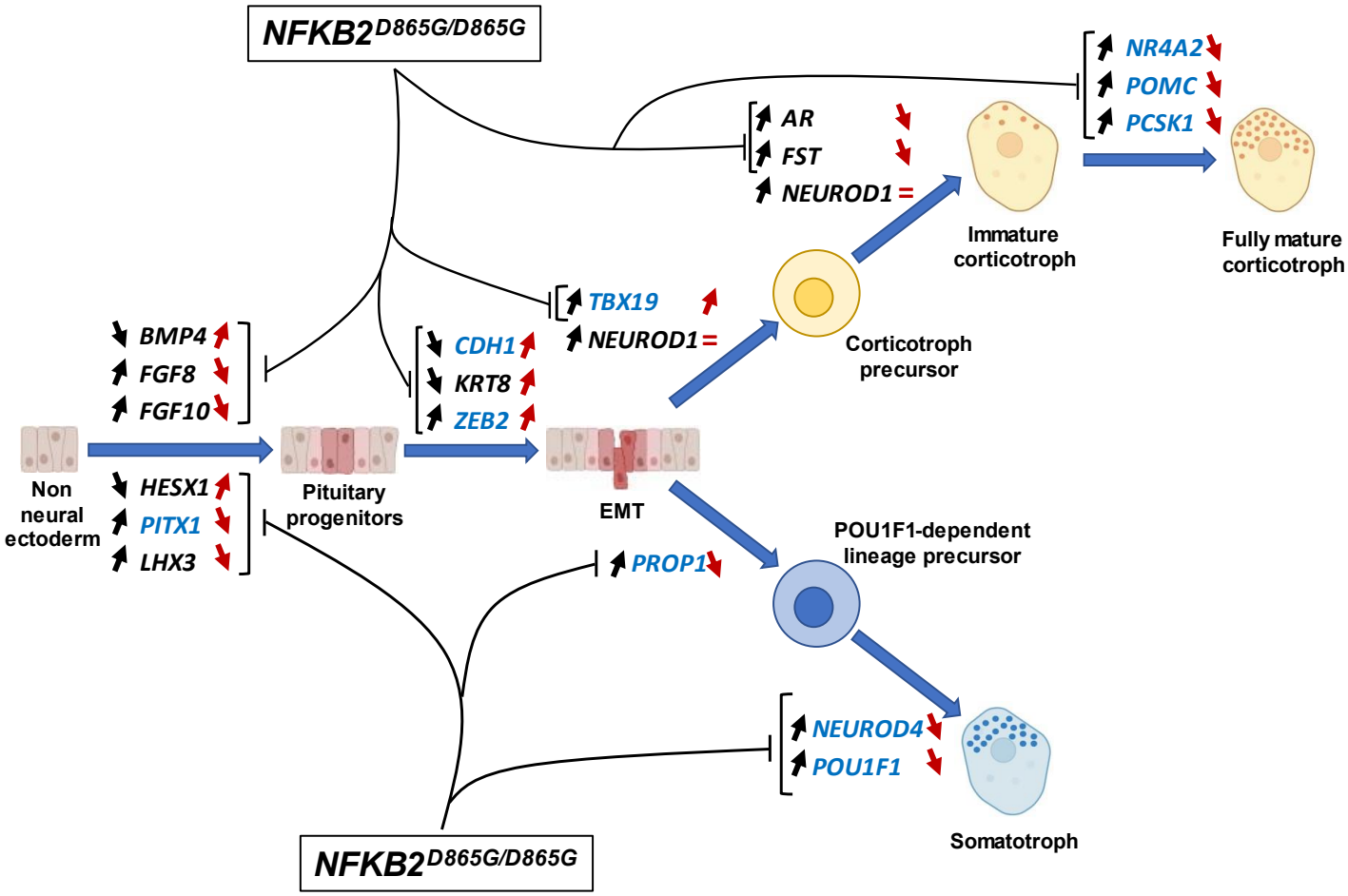
NFKB2D865G/D865G
NR4A2
POMC
PCSK1
AR
FST
NEUROD1 =
Immature corticotroph
Fully mature corticotroph
TBX19
NEUROD1 =
Corticotroph precursor
BMP4
FGF8
FGF10
CDH1
KRT8
ZEB2
Non neural ectoderm
HESX1
PITX1
LHX3
Pituitary progenitors
EMT
PROP1
POU1F1-dependent lineage precursor
NEUROD4
POU1F1
Somatotroph
NFKB2D865G/D865G

gene_name	FoldChange	padj	gene_name	FoldChange	padj	gene_name	FoldChange	padj
ADCYAP1	0,447	0,0079	GLI3	1,279	0,1009	PITX2	1,072	0,8669
AIP	0,898	0,5344	GNAS	1,058	0,3952	POLR3A	1,014	0,9072
ALDH1A1	0,153	1,258E-09	GNRHR	0,453	0,0001	POMC	0,434	0,0036
ALDH1A2	0,152	4,598E-05	GNRHR2	0,698	0,2394	POU1F1	0,039	0,0007
ALDH1A3	0,182	2,61E-13	GPR101	1,209	0,8305	POU3F1	1,374	0,4209
AR	0,634	0,0017	GREB1	1,007	0,9778	POU3F2	0,266	1,3628E-05
ARNT2	0,534	0,0003	GSX1	0,659	0,4501	POU5F1	3,573	0,1702
ASCL1	0,345	1,44E-06	HES1	0,663	0,0280	PROKR2	1,056	0,9737
AXIN2	1,296	0,0589	HESX1	2,193	0,0312	PROP1	0,054	0,0007
BMP2	0,750	0,3428	HEY1	0,804	0,1305	RAX	0,599	0,0270
BMP4	4,357	2,4368E-05	HMGA2	0,775	0,1947	RBPJ	0,814	0,0466
BMPR1A	1,019	0,9199	INHBB	0,458	0,0397	S100B	0,304	2,1550E-05
BRAF	0,892	0,4818	ISL1	1,097	0,7581	SALL1	1,106	0,7612
CDH1	1,626	0,0090	KRT8	2,617	1,99E-06	SHH	0,786	0,5118
CGA	12,756	0,0423	LATS1	0,857	0,0200	SIX1	0,219	8,42E-06
CREB1	0,850	0,1290	LATS2	1,460	0,0166	SIX2	0,161	8,97E-09
CRH	4,347	0,0047	LHX2	0,622	0,0062	SIX3	0,859	0,6998
CRHR1	0,156	0,0513	LHX3	0,064	2,39E-06	SIX6	0,467	0,0059
CRHR2	0,823	0,7360	LHX4	0,557	0,0040	SLC15A2	0,624	0,0016
CTNNB1	1,009	0,9554	MEN1	1,030	0,8031	SLC6A3	2,215	0,1580
CYP11A1	6,086	0,0017	MSX1	0,904	0,9091	SMO	0,957	0,7040
DIO2	1,114	0,7189	NANOG	6,301	0,0047	SMOC2	4,163	0,0349
DISP1	1,142	0,4771	NEUROD1	0,883	0,5097	SOX11	0,736	0,1276
DLK1	0,594	0,0199	NEUROD2	1,137	0,8418	SOX2	0,815	0,4215
DMRTA2	0,144	3,58E-11	NEUROD4	0,320	1,7211E-05	SOX3	0,787	0,5015
DRD2	2,753	2,0454E-05	NEUROG1	0,493	0,1921	SOX9	0,557	0,0021
DUOX2	2,595	0,0196	NEUROG2	0,208	0,0317	SRD5A1	0,961	0,7979
DZIP1	0,818	0,0426	NFKB2	1,236	0,1614	SST	0,994	0,9921
EGR1	1,784	0,1577	NKX2-1	0,707	0,1552	SSTR1	0,509	0,0901
EPCAM	1,128	0,7273	NKX2-2	1,569	0,3732	SSTR2	0,769	0,4360
ETS1	3,947	4,82E-13	NOG	1,376	0,3190	TAZ	0,967	0,8532
EYA1	0,514	0,0396	NOTCH1	1,006	0,9829	TBX19	0,663	0,0129
FGF10	0,267	3,49E-09	NOTCH2	0,937	0,6069	TBX3	0,997	0,9891
FGF2	1,224	0,1824	NR0B1	1,062	0,9289	TCF4	1,015	0,9577
FGF3	0,611	0,0844	NR3C1	0,846	0,3028	TCF7L2	1,178	0,5884
FGF8	0,506	0,0483	NR4A1	1,227	0,6213	TFAP2A	2,887	0,0017
FOLR1	2,729	0,0344	NR4A2	0,407	0,0008	TGIF1	1,422	0,0028
FOXA1	0,550	0,0219	NR5A1	0,834	0,6140	THRA	0,714	0,0071
FOXC1	1,619	0,1182	NUPR1	1,384	0,3477	THRB	2,260	0,0002
FOXJ1	0,424	0,0012	OLFM1	0,830	0,2917	TIPRL	0,810	0,0039
FOXO1	1,494	0,0078	OTP	0,663	0,1935	TLE5	0,695	0,0050
FST	2,384	9,05E-06	OTX1	0,863	0,7223	TSHR	0,998	0,9975
GATA2	5,579	9,69E-11	OTX2	0,976	0,9471	USP39	1,035	0,7908
GATA3	4,758	0,0048	PAX3	0,362	0,1196	WNT4	0,712	0,1166
GHRH	0,712	0,6505	PAX6	0,294	0,0006	WNT5A	1,442	0,2954
GHRHR	0,672	0,4851	PAX7	0,570	0,1882	YAP1	1,091	0,5659
GLI1	1,050	0,8410	PCSK1	0,354	0,0003	ZBTB20	0,354	5,29E-10
GLI2	1,328	0,1593	PITX1	0,299	6,27E-07	ZEB2	1,378	0,0108

Stemness markers			Epithelial markers			Mesenchymal markers		
Gene	**fold change**	**padj**	**Gene**	**fold change**	**padj**	**Gene**	**fold change**	**padj**
SOX2	0,815	0,4215	**CDH1**	1,626	0,0090	**CDH2**	0,616	0,0003
SOX4	0,784	0,0245	**EPCAM**	1,128	0,7273	**SNAI1**	3,379	7,14E-06
SOX9	0,557	0,0021	**KRT8**	2,617	1,9871E-06	**VIM**	0,663	0,0366
NOTCH2	0,937	0,6069	**CLDN4**	1,203	0,3140	**COL2A1**	1,662	0,0849
HES1	0,663	0,0280	**GRHL2**	1,360	0,1920	**COL1A1**	10,939	7,7645E-06